PCCP

Cite this: *Phys. Chem. Chem. Phys.*, 2011, **13**, 13926–13941

www.rsc.org/pccp

PAPER

Structures and IR/UV spectra of neutral and ionic phenol–Ar_n cluster isomers ($n \leq 4$): competition between hydrogen bonding and stacking†‡

Matthias Schmies,[a] Alexander Patzer,[a] Masaaki Fujii[b] and Otto Dopfer*[a]

Received 8th March 2011, Accepted 19th April 2011
DOI: 10.1039/c1cp20676a

The structures, binding energies, and vibrational and electronic spectra of various isomers of neutral and ionic phenol–Ar_n clusters with $n \leq 4$, $PhOH^{(+)}$–Ar_n, are characterized by quantum chemical calculations. The properties in the neutral and ionic ground electronic states (S_0, D_0) are determined at the M06-2X/aug-cc-pVTZ level, whereas the S_1 excited state of the neutral species is investigated at the CC2/aug-cc-pVDZ level. The Ar complexation shifts calculated for the S_1 origin and the adiabatic ionisation potential, ΔS_1 and ΔIP, sensitively depend on the Ar positions and thus the sequence of filling the first Ar solvation shell. The calculated shifts confirm empirical additivity rules for ΔS_1 established recently from experimental spectra and enable thus a firm assignment of various S_1 origins to their respective isomers. A similar additivity model is newly developed for ΔIP using the M06-2X data. The isomer assignment is further confirmed by Franck–Condon simulations of the intermolecular vibrational structure of the $S_1 \leftarrow S_0$ transitions. In neutral PhOH–Ar_n, dispersion dominates the attraction and π-bonding is more stable than H-bonding. The solvation sequence of the most stable isomers is derived as (10), (11), (30), and (31) for $n \leq 4$, where (*km*) denotes isomers with *k* and *m* Ar ligands binding above and below the aromatic plane, respectively. The π interaction is somewhat stronger in the S_1 state due to enhanced dispersion forces. Similarly, the H-bond strength increases in S_1 due to the enhanced acidity of the OH proton. In the $PhOH^+$–Ar_n cations, H-bonds are significantly stronger than π-bonds due to additional induction forces. Consequently, one favourable solvation sequence is derived as (H00), (H10), (H20), and (H30) for $n \leq 4$, where (H*km*) denotes isomers with one H-bound ligand and *k* and *m* π-bonded Ar ligands above and below the aromatic plane, respectively. Another low-energy solvation motif for $n = 2$ is denoted $(11)^H$ and involves nonlinear bifurcated H-bonding to both equivalent Ar atoms in a C_{2v} structure in which the OH group points toward the midpoint of an Ar_2 dimer in a T-shaped fashion. This dimer core can also be further solvated by π-bonded ligands leading to the solvation sequence (H00), $(11)^H$, $(21)^H$, and (22) for $n \leq 4$. The implications of the ionisation-induced π → H switch in the preferred interaction motif on the isomerisation and fragmentation processes of $PhOH^{(+)}$–Ar_n are discussed in the light of the new structural and energetic cluster parameters.

1. Introduction

Isolated clusters of phenol (PhOH) with rare gas (Rg) atoms are suitable benchmark model systems to study the subtle competition between different intermolecular binding motifs at the molecular level using sophisticated experimental and theoretical techniques.[1–5] The Rg atoms can either bind to the acidic OH group *via* H-bonding (H-bond) or to the aromatic π-electron system *via* dispersive stacking interactions (π-bond). These binding motifs are frequently referred to as hydrophilic and hydrophobic interactions, respectively.[1,4,6] The preference for a specific binding motif and the resulting interaction strength depends sensitively on many parameters, such as the electronic excitation and charge or protonation state, the substitution of functional groups, the type of ligand, and the size of the cluster.[3–5,7–11] Neutral PhOH–Rg dimers prefer π-bonding because dispersion dominates the attraction, whereas $PhOH^+$–Rg cations prefer H-bonding because the additional charge-induced polarisation forces provide substantial further stabilisation.[12,13] This charge-induced π → H switch is a general phenomenon for acidic aromatic molecules interacting

[a] *Institut für Optik und Atomare Physik, Technische Universität Berlin, 10623 Berlin, Germany. E-mail: dopfer@physik.tu-berlin.de*
[b] *Chemical Resources Laboratory, Tokyo Institute of Technology, Yokohama 226-8503, Japan*

† Dedicated to Bernhard Brutschy on the occasion of his 65th birthday.

‡ Electronic supplementary information (ESI) available. See DOI: 10.1039/c1cp20676a

with nonpolar ligands,[4] and has been established for a variety of aromatic molecules with acidic OH or NH functional groups, including phenol,[12–18] resorcinol,[19] naphthol,[20] aniline,[21–23] indole,[24] and imidazole.[25]

The present work characterizes the structures, binding energies, and vibrational and electronic spectra of various isomers of neutral and ionic $PhOH^{(+)}$–Ar_n clusters with $n \leq 4$ by quantum chemical calculations in three different electronic states, namely the neutral ground and first excited singlet states (S_0, S_1) and the cation ground state (D_0). To this end, we review the current knowledge on these systems relevant for the present work. For this purpose, we employ the following nomenclature for the various $PhOH^{(+)}$–Ar_n isomers (Fig. 1). Consistent with the previous notation, ($k|m$) or (km) describes an isomer with $n = k + m$ π-bound ligands, in which k and m Ar atoms are located above and below the aromatic plane, respectively. In the case of a single additional H-bound ligand, the notation is extended to (Hkm).

A large number of spectroscopic[3,7,26–33] and advanced quantum chemical studies[29,34–36] demonstrate that neutral PhOH–Ar has a π-bonded (10) equilibrium structure in S_0. Fig. 2 reproduces the two-color resonance-enhanced two-photon ionisation (REMPI) spectra of the $S_1 \leftarrow S_0$ electronic transition of PhOH–Ar_n for n = 0–4.[37] Hole-burning experiments show that all bands observed in the $n = 1$ spectrum arise from a single isomer, featuring an intense S_1 origin band (0^0) with a complexation-induced redshift of $\Delta S_1 = -34\ cm^{-1}$ and minor intermolecular excitation.[31] Analysis of recent rotationally-resolved laser-induced fluorescence (LIF) spectra of the $S_1 0^0$ band proves that this isomer has indeed a (10) structure.[29] The experimental dissociation energy derived for (10) from mass-analyzed threshold ionisation (MATI), $D_0 = 364 \pm 13\ cm^{-1}$, is consistent with the best theoretical value of 389 cm^{-1} calculated at the CCSD(T)/CBS level.[36] The H-bonded (H00) isomer is predicted to be substantially less stable than (10) and has not yet been detected experimentally. At the present stage, it is unclear whether (H00) is a shallow local minimum on the PhOH–Ar potential or a transition state connecting the two global (10) minima *via* a barrier of the order of 250 cm^{-1}.[34,36] Other binding sites, such as H-bonding to the CH groups are less stable and thus not considered further.[34,35]

Similar to the $n = 1$ complex, hole-burning spectroscopy reveals that the $n = 2$ REMPI spectrum in Fig. 2 is dominated

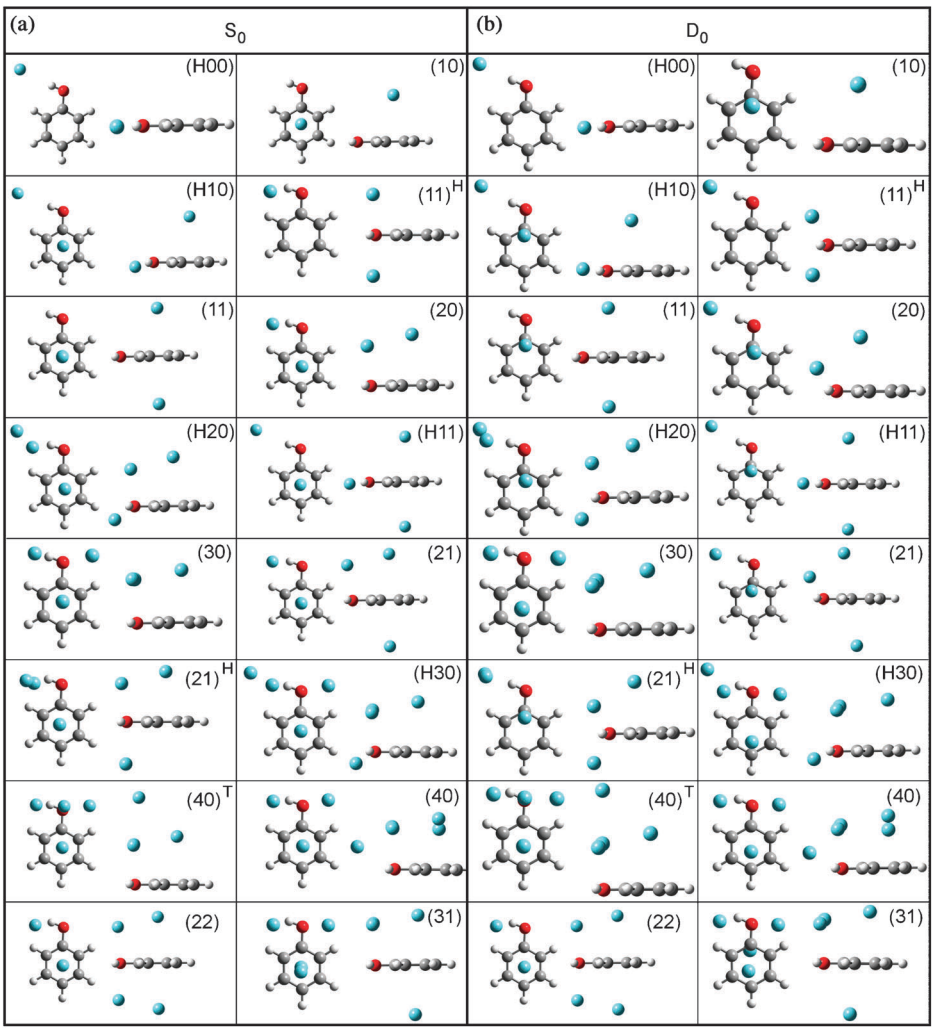

Fig. 1 (a) Structures of various isomers of PhOH–Ar_n in the S_0 state calculated at the M06-2X/aug-cc-pVTZ level. (b) Structures of various isomers of cationic $PhOH^+$–Ar_n in the D_0 state calculated at the M06-2X/aug-cc-pVTZ level.

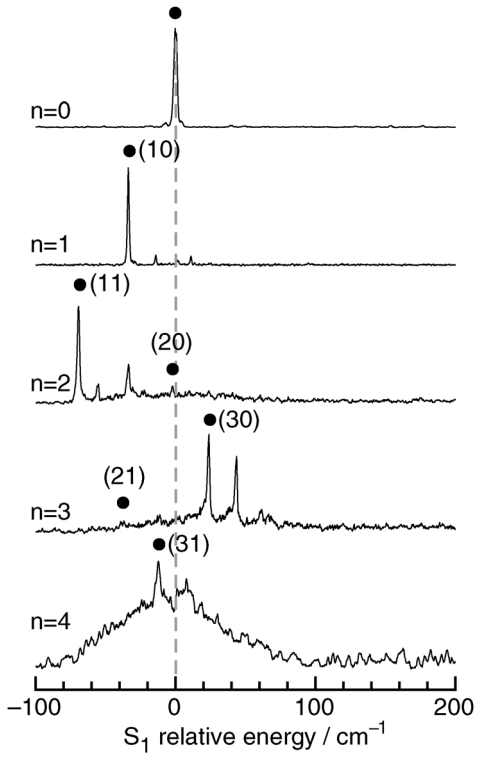

Fig. 2 Two-color REMPI spectra of PhOH–Ar$_n$ with $n \leq 4$ recorded in the vicinity of the S_1 origin of PhOH at 36 350 cm^{-1}, which is set as the reference frequency ($\Delta S_1 = 0$).[37] The S_1 origins are indicated by filled circles (Table 3).

by a single isomer with an S_1 origin at $\Delta S_1 = -69$ cm^{-1},[31] which was later firmly identified as the (11) isomer by rotationally-resolved LIF spectroscopy.[29] The total binding energy of (11) for loss of both Ar ligands, extracted from its MATI spectrum as $\sim$775 cm^{-1}, is about twice as large as that of (10). This result is consistent with the almost additive ΔS_1 redshifts arising from the nearly equivalent Ar atoms in (10) and (11),[29] and provides the basis for the additivity model.[37,38] In contrast to the $n = 1$ complex, high-level *ab initio* calculations are lacking for $n = 2$. Calculations at moderate theoretical levels are however consistent with this assignment.[29,31,39] Although spectra of the related benzene–Ar$_2$ and aniline–Ar$_2$ clusters exhibit also significant signals from a less stable (20) structure, this type of isomer has escaped identification in the PhOH–Ar$_2$ spectra for a long time owing to its weak intensity in most REMPI spectra. Only very recently, an empirical additivity model developed for the ΔS_1 shifts of PhOH–Ar$_n$ suggested a tentative assignment of the S_1 origin of (20) to a weak transition at $\Delta S_1 = -2$ cm^{-1} (Fig. 2).[37] This interpretation requires, however, further spectroscopic and/or quantum chemical support.

Reliable information on the structures of the $n = 3$ and $n = 4$ clusters in S_0 is not available, because high-resolution spectra and detailed quantum chemical calculations are lacking. Only vibrationally-resolved IR and UV spectra were reported,[37,39,40] and the REMPI spectra are shown in Fig. 2.[37] Photoionisation efficiency (PIE) and photofragmentation studies of the $n = 3$ complex demonstrate that all Ar ligands are π-bonded in the isomer responsible for the intense S_1 origin at $\Delta S_1 = +23$ cm^{-1}.[41] Hole-burning spectra reveal that all intense bands in these spectra are due to intermolecular structure of this isomer.[31] The interpretation of its geometry has, however, been conflicting so far. Initial assignments suggested a (21) structure,[40,42] whereas the recent application of the additivity model concluded a (30) structure.[37] The latter model also led to the new identification of the weak S_1 origin of the (21) isomer at $\Delta S_1 = -37$ cm^{-1}.[37] Again, both tentative assignments call for further spectroscopic and/or quantum chemical confirmation. The $n = 4$ spectrum in Fig. 2 displays an intense S_1 origin at $\Delta S_1 = -12$ cm^{-1}, which according to the additivity model was attributed to the (31) isomer,[37] in conflict with a recent interpretation as (40).[39,43] The origin of the broad background in the $n = 4$ spectrum is unclear. It may arise from fragmentation of larger clusters ($n \geq 5$) or spectral congestion due to signals from other $n = 4$ isomers. During the course of the present work, REMPI spectra of $n = 5$ and $n = 6$ were reported, and weak peaks on top of a broad and largely unstructured signal at $\Delta S_1 = -20$ and -44 cm^{-1} were interpreted as S_1 origins of (50) and (60) isomers by comparison with corresponding shifts of aniline–Ar$_n$, although calculations suggested structures with solvation on both sides to be more stable.[39] This discrepancy was attributed to expansion conditions favouring the production of PhOH–Ar$_n$ clusters with single-sided Ar solvation for the size range $n \geq 3$.[39]

Due to the multiple binding sites for Ar to PhOH, the number of possible low-energy isomers of PhOH–Ar$_n$ increases rapidly with n. Spectroscopy of PhOH–Ar$_n$ in a cold supersonic molecular beam at temperatures of $T < 10$ K reveals, however, the presence of only a few isomers, at least in the size range $n \leq 3$.[29,31] The PhOH–Ar$_n$ clusters produced in the molecular beam are relatively rigid and thus solid-like. For example, molecular dynamics simulations for the related benzene–Ar$_2$ complex illustrate that isomerisation processes of the type (11) $\leftrightarrow$ (20) *via* substantial barriers become only relevant for $T > 40$ K (melting).[44] As the binding energies and potential barriers for Ar clusters interacting with PhOH and benzene are of similar magnitude, the melting temperatures for both cluster systems are expected to be similar, too. Interestingly, the simulations reveal that at temperatures above melting and below boiling (evaporation) the less stable (20) isomer of benzene–Ar$_2$ is more abundant than the more stable (11) isomer due to entropy.[44]

Spectroscopic[12,13,15] and theoretical studies[12,14,35,45] show that in the cationic D_0 state the H-bonded (H00) structure is the global minimum on the PhOH$^+$–Ar potential and more stable than the π-bonded (10) local minimum. The dissociation energies of $D_0 \approx 900$ and 535 ± 3 cm^{-1} measured for (H00)[41,46] and (10)[47] are compatible with the interaction energies of 946 and 595 cm^{-1} obtained at the CCSD(T)/CBS level, respectively.[45] As ionisation of PhOH–Ar switches the energetic order of the π and OH binding sites, all spectroscopic techniques based on photoionisation of the neutral (10) global minimum generated in the molecular beam initially prepare only the (10) local minimum of the cation due to vertical Franck–Condon (FC) transitions and provide thus mainly spectroscopic information about this less stable isomer. In contrast, electron ionisation (EI) generates predominantly the most stable PhOH$^+$–Ar$_n$ isomers.[4,48] The IR spectra of these

$PhOH^+$–Ar_n clusters were interpreted with a solvation sequence in which the initially formed (H00) dimer is further solvated by $n - 1$ π-bound ligands.[13] However, the preferred distribution of the π-bonded ligands above and below the aromatic ring has remained unclear and is one of the topics in the present study. The ionisation-induced π → H switch in the most stable binding motif in $PhOH^{(+)}$–Ar_n leads to interesting photoionisation and photofragmentation energetics, which were investigated in some detail for $n = 2$ and 3.[41,46] These experiments provide information about the dissociation energies of the (11) and (30) clusters in all three considered electronic states (D_0, S_1, S_0) using appearance energies for fragmentation in the D_0 state and spectral ΔS_1 and ΔIP shifts, although the position of the π-bonded Ar atoms in $n = 3$ was not specified. The π → H isomerisation processes triggered by ionisation were recently characterized in real time by picosecond time-resolved IR spectroscopy for the (11) isomer of PhOH–Ar_2,[6,32,49] the (30) isomer of PhOH–Ar_3,[37] and the (10) isomer of PhOH–Kr,[50] demonstrating that the dynamical behaviour strongly depends on the mass and number of the Rg atoms, with respect to both the isomerisation mechanism and the corresponding rate constants.

The present work aims at the quantum chemical characterization of the structures, binding energies, and vibrational and electronic spectra of isomeric PhOH–Ar_n clusters with $n \leq 4$ in the S_0, S_1, and D_0 states with the following major objectives. (1) Initially, the structures and interaction energies of neutral PhOH–Ar_n isomers are evaluated at the M06-2X/aug-cc-pVTZ level to establish the most stable structures of each cluster size. The results will enable us to determine the isomers, which are populated in the molecular beam and give rise to the experimental IR and UV spectra. These are the first quantum chemical calculations providing reliable information about the cluster growth sequence in PhOH–Ar_n up to the size $n = 4$. The chosen theoretical level is based on density functional theory (DFT) and accounts for the important dispersion forces.[51,52] Moreover, it is sufficiently efficient to explore larger clusters and it reproduces all available binding energies to satisfactory accuracy. (2) In a subsequent effort, the $S_1 \leftarrow S_0$ excitation spectra of all relevant isomers are calculated at the RI-CC2/aug-cc-pVDZ level. The major goal of these calculations is the confirmation of the empirically established additivity model for the ΔS_1 origin shifts and to provide a firm assignment of these origins to the corresponding cluster structures. These calculations are supplemented by harmonic FC simulations of the intermolecular vibrational structure in S_1, which provide further support for the given isomer assignment. It will be demonstrated that this theoretical level is suitable to efficiently provide a reliable description of the electronically excited states of these weakly-bound clusters. (3) Finally, the structures and binding energies of the ionic $PhOH^+$–Ar_n isomers are calculated at the M06-2X/aug-cc-pVTZ level to evaluate the effects of the excess charge on the intermolecular interactions and the cluster growth sequence. In particular, we establish an additivity model for the ΔIP shifts similar to the one developed recently for ΔS_1. These are the first quantum chemical calculations for the cation clusters with $n = 2$–4 and they provide reliable information about the cluster growth sequence in this size regime. A further motivation for these calculations is to derive structural assignments for the isomers observed in IR photodissociation (IRPD) spectra of $PhOH^+$–Ar_n clusters generated in the EI source.[13] In addition, the results will provide clues about the $PhOH^+$–Ar_m product isomers ($m \leq n$), which are experimentally observed upon ionisation of the neutral PhOH–Ar_n precursors after the isomerisation and fragmentation processes.[6,32,37,41,46]

2. Theoretical techniques

The geometric, energetic, and vibrational properties of PhOH–Ar_n isomers with $n \leq 4$ are determined in the neutral and cationic ground electronic states (S_0, D_0) at the M06-2X/aug-cc-pVTZ level using GAUSSIAN09 (version A.02).[53] This DFT functional accounts for dispersion,[51,52] which is particularly important for the interaction between Ar ligands and also their interaction with the π electrons of the aromatic ring. For this reason, traditional DFT functionals without dispersion, such as the popular B3LYP functional, are not suitable.[12] On the other hand, MP2 calculations account for most of the dispersion energy but severely suffer from spin contamination in calculations of the open-shell $PhOH^+$–Ar_n cation clusters. For example, $S^2 - 0.75 > 0.18$ is obtained for $PhOH^+$ at the unrestricted MP2/6-311G(2df,2pd) level. In contrast, the M06-2X/aug-cc-pVTZ level does not suffer from spin contamination (*e.g.*, $S^2 - 0.75 < 0.03$ for $PhOH^+$). It also reproduces the PhOH–Ar interaction energies in both charge states for both relevant principal binding sites, namely stacking and hydrogen bonding, as is evidenced by the satisfactory agreement between calculated and experimental dissociation energies (Table 1). Moreover, also the experimentally derived Ar–Ar interaction of $D_e = 99$ cm^{-1} is reproduced with sufficient accuracy at this level ($D_e = 82$ cm^{-1}). Thus, the M06-2X/aug-cc-pVTZ approach provides an efficient but

Table 1 Binding energies (D_e and D_0 in cm^{-1}) for the H-bonded (H00) and π-bonded (10) isomers of PhOH–Ar in the S_0 and D_0 electronic states evaluated at various theoretical levels compared to available experimental data

	S_0 (H00)	S_0 (10)	D_0 (H00)	D_0 (10)
Exp.[a]		364 ± 13	~870 650 ± 150	535 ± 3
B3LYP/6-311G**[b]			444 (D_0)	
DFT-B97-D/def2-TZVP[c]		316 (D_e)		
MP2/6-31G*[d]			332 (D_e)	83 (D_e)
MP2/aug-cc-pVDZ[e]	205 (D_e)	371 (D_0) 420 (D_e)		
MP2/6-311G(2df,2pd)[f]			685 (D_e)	415 (D_e)
MP2/6-311++G(3df,2pd)[g]		493 (D_0)	836 (D_0)	
MP2/CBS[g]		577 (D_0)	836 (D_0)	
CCSD(T)/CBS[h]	285 (D_e)	389 (D_0) 434 (D_e)	946 (D_e)	542 (D_0) 595 (D_e)
M06-2X/6-311+G(d,p)[i]	110 (D_0) 125 (D_e)	385 (D_0) 439 (D_e)	557 (D_0) 562 (D_e)	498 (D_0) 532 (D_e)
M06-2X/aug-cc-pVTZ[i]	69 (D_0) 158 (D_e)	317 (D_0) 382 (D_e)	744 (D_0) 805 (D_e)	492 (D_0) 571 (D_e)
RI-CC2/aug-cc-pVDZ[i]	383 (D_0) 493 (D_e)	623 (D_0)[j] 675 (D_e)[j]		

[a] D_0 values from ref. 13, 41 and 47. [b] Ref. 16. [c] Ref. 29. [d] Ref. 12. [e] Ref. 34. [f] Ref. 15. [g] Ref. 35. [h] Ref. 36 and 45. [i] Present work. [j] Including BSSE: $D_e = 432$ cm^{-1}, $D_0 = 394$ cm^{-1}.

reliable tool to evaluate the potential energy surface of larger PhOH–Ar$_n$ clusters with satisfactory confidence. In general, all coordinates are relaxed for the search of stationary points on a potential energy surface, which is corrected for basis set superposition error (BSSE). Vibrational analysis is used to establish the nature of the stationary points as minimum or transition state. Interaction energies (D_e) are corrected for harmonic zero-point energies (ZPE) to yield binding energies (D_0). The O–H stretching frequencies are scaled by a factor of 0.9407 and 0.9452 for the S_0 and D_0 states to match the calculated and experimental frequencies of PhOH$^{(+)}$ in the two electronic states (3658 and 3534 cm^{-1}),[30,37] respectively.

Evaluation of adiabatic $S_1 \leftarrow S_0$ transition energies and selected properties of the S_0 and S_1 electronic states is carried out for all relevant PhOH–Ar$_n$ isomers using TURBOMOLE (version 6.1).[54] Full geometry optimisation of the S_0 and S_1 states is performed using the RI-CC2 approach. As a compromise between accuracy and computational expense, the aug-cc-pVDZ basis set is used for all calculations at this level. The RI-CC2/aug-cc-pVDZ model was shown to provide reliable transition energies for electronic $S_1 \leftarrow S_0$ transitions of closed-shell aromatic molecules and their clusters with weakly bound ligands.[55,56] All coordinates are relaxed for the search of stationary points in S_0 and S_1. Vibrational frequencies and harmonic ZPE in both electronic states are calculated from numerical derivatives of the analytical RI-CC2 gradient to correct the adiabatic $S_1 \leftarrow S_0$ transition energies for ZPE. If not stated otherwise, the RI-CC2 energies are not corrected for BSSE.

Franck–Condon simulations of the $S_1 \leftarrow S_0$ transitions are performed using PGOPHER (version 7.1.108).[57] The simulations employ harmonic vibrational frequencies and geometries for the S_0 and S_1 states obtained from the RI-CC2/aug-cc-pVDZ calculations. Only intermolecular modes are considered, because only these are observed in the experimental spectra discussed here. All FC simulations are carried out for $T = 0$ K to establish the assignments of the principal vibrational transitions. This choice is justified, as the experimental $S_1 \leftarrow S_0$ REMPI spectra do not show any hot bands due to the low vibrational temperature in the molecular beam expansion.

3. Results and discussion

3.1 S_0 state

Optimised equilibrium structures of various PhOH–Ar$_n$ isomers in the S_0 state obtained at the M06-2X/aug-cc-pVTZ level are shown in Fig. 1. Similar geometries are derived at the RI-CC2/aug-cc-pVDZ level. The total stabilisation and binding energies (D_e and D_0) for the process nAr + PhOH $\rightarrow$ PhOH–Ar$_n$ calculated at both levels are listed in Table 2. Table 1 compares the interaction energies for the H-bonded and π-bonded isomers of PhOH$^{(+)}$–Ar with available experimental binding energies and theoretical values obtained previously at a variety of quantum chemical levels. Significantly, the D_0 values derived at the M06-2X/aug-cc-pVTZ level underestimate only slightly but systematically the experimental D_0 energies in both the neutral and ionic ground electronic state by 10–20%. This result demonstrates that this level provides a reliable representation of the PhOH$^{(+)}$–Ar interaction in the two charge states for both the stacking and H-bonding motifs. The agreement between calculated interaction energies D_e and measured D_0 values is even better, with deviations of less than 8%. Apparently, the ZPE is substantially overestimated using the harmonic approach for the intermolecular modes, and this deficiency becomes more pronounced for the larger clusters. For this reason, the theoretical D_e values are compared to the measured D_0 values in Fig. 3 and throughout the manuscript (although both values are listed in the tables). As the Ar–Ar interaction at the M06-2X/aug-cc-pVTZ level is also close to experiment (82 *vs.* 99 cm^{-1}),[58] the M06-2X/aug-cc-pVTZ level is considered as an efficient but reliable method for describing the properties of the larger PhOH$^{(+)}$–Ar$_n$ clusters with $n \leq 4$ in S_0 and D_0. Closer inspection of Table 1 also reveals that MP2 calculations with small basis sets strongly underestimate the stacking interaction in PhOH–Ar, whereas the value at the CBS limit is far too large when compared to experiment (D_0 = 577 *vs.* 364 cm^{-1}).

In the following, we discuss the properties of the PhOH–Ar$_n$ isomers in the S_0 state at the M06-2X level (Fig. 1 and 3a, Table 2). The π-bonded (10) isomer corresponds to the global minimum on the potential energy surface of the n = 1 complex, as dispersion forces between Ar and the highly polarisable π electrons of the aromatic ring dominate the attraction. The calculated interaction energy of 382 cm^{-1} compares well with the measured value of 364 ± 13 cm^{-1}.[47] Also, the rotational constants (A_e = 1850 MHz, B_e = 1191 MHz, C_e = 970 MHz) are close to the experimental values (A_0 = 1819 MHz, B_0 = 1125 MHz, C_0 = 918 MHz).[29] The Ar atom is slightly displaced from the centre of the aromatic ring toward the OH substituent (x_e = 0.50 Å), with an Ar-ring separation of R_e = 3.40 Å. This separation is somewhat smaller than the experimental value of R_0 = 3.53 Å,[29] which is partly due to zero-point excursion in the ground vibrational state ($\Delta R \approx 0.05$ Å).[34] The three harmonic intermolecular frequencies ω_i = 33 (b_x), 55 (b_y), and 63 cm^{-1} (s_z) are significantly larger than the calculated fundamental frequencies estimated at the MP2/aug-cc-pVDZ level (ν_i = 21, 35, and 45 cm^{-1}),[34] and the ratio of $\nu_i/\omega_i \approx 0.7$ is a suitable scaling factor to account for anharmonicity.

The planar H-bound (H00) structure with C_s symmetry is significantly less stable than (10), and the nearly linear H-bond is characterized by D_e = 158 cm^{-1}, R_{H-Ar} = 2.70 Å, θ_{O-H-Ar} = 175.6°, and an intermolecular stretch frequency of 47 cm^{-1}. At present, it is unclear whether (H00) is a shallow local minimum or a transition state.[34,36,45] At the M06-2X/aug-cc-pVTZ level, (H00) is a minimum with intermolecular frequencies of ω_i = 12, 23, and 47 cm^{-1}. In general, the geometric and energetic parameters of the H-bound and π-bound minima are similar to those derived at more sophisticated, state-of-the-art *ab initio* calculations.[34,36]

Four principal minimum structures are calculated for PhOH–Ar$_2$ (Fig. 1, Table 2). The (11) isomer with C_s symmetry and two equivalent π-bonded Ar ligands is the global minimum in S_0. The total dissociation energy of 757 cm^{-1} agrees well with the experimental value of ~775 cm^{-1}.[46] Moreover, it is nearly twice the interaction energy of (10), indicating that there is little interaction in (11) between the two

Table 2 Interaction (D_e) and binding (D_0, in parentheses) energies for various PhOH–Ar_n isomers in three electronic states evaluated at the M06-2X/aug-cc-pVTZ and RI-CC2/aug-cc-pVDZ levels compared to available experimental D_0 values (in cm^{-1})

n	Isomer	S_0 M06-2X	S_0 Exp[a]	S_0 RI-CC2	S_1 RI-CC2	S_1 Exp[a]	D_0 M06-2X	D_0 Exp[a]
1	(H00)	158		493	550		805	~870
		(69)		(383)	(437)		(744)	
	(10)	382	364 ± 13	675[b]	780	397 ± 13	571	535 ± 3
		(317)		(623[b])	(692)		(492)	
2	(H10)	548					1359	
		(415)					(1217)	
	(20)	719		1265	1331		1338	
		(500)		(1156)	(1181)		(1132)	
	(11)	757	775 ± 75	1410	1620	844 ± 75	1097	1115 ± 65
		(530)		(1285)	(1433)		(951)	
	$(11)^H$	465					1384	
		(257)					(1175)	
3	(H20)	990					2043	
		(716)					(1697)	
	(H11)	929					1893	
		(672)					(1632)	
	(30)	1083	1179 ± 45	1958	1958	1154 ± 45	1671	1730 ± 30
		(799)		(1770)	(1750)		(1378)	
	(21)	1075		2014	2189		1850[c]	
		(868)		(1842)	(1947)		(1587)	
	$(21)^H$	934[c]					2033	
		(678)					(1726)	
4	(H30)	1374					2502	
		(977)					(2048)	
	(H21)	1339					2495[c]	
		(1045)					(2194)	
	(40)	1422		2590	2624		2134	
		(1024)		(2342)	(2349)		(1786)	
	$(40)^T$	1313					1924	
		(1035)					(1581)	
	(31)	1446		2745	2856		2187	
		(1068)		(2489)	(2556)		(1888)	
	(22)	1419		2674	2835		2663	
		(1038)		(2424)	(2522)		(2168)	

[a] Ref. 41, 46, 47 and 62. Experimental binding energies for $n = 2$ and 3 in S_0 and S_1 are derived from those measured in D_0 by taking experimental ΔS_1 and ΔIP shifts into account. [b] Including BSSE: $D_e = 432\ cm^{-1}$, $D_0 = 394\ cm^{-1}$. [c] Transition state (no local minimum found).

Ar ligands located on opposite sides of the PhOH plane. This view is confirmed by the geometrical parameters. For example, the Ar-ring separation increases by 0.01 Å upon addition of the second Ar ligand, which is consistent with the experimental result estimated from the analysis of the rotational constants (0.02 Å).[29] There is essentially no further shift toward the OH group ($\Delta x_e = 0.02$ Å). The calculated rotational constants ($A_e = 1765$ MHz, $B_e = 495$ MHz, $C_e = 447$ MHz) are also close to the experimental ones ($A_0 = 1778$ MHz, $B_0 = 463$ MHz, $C_0 = 421$ MHz).[29] The six intermolecular frequencies of $\omega_i/cm^{-1} = 28$ (b_{xs}), 33 (b_{ys}), 55 (b_{xa}), 70 (s_{zs}), 92 (b_{ya}), and 101 (s_{za}) are again substantially larger than available experimental fundamental frequencies (measured in S_1).[31,40]

The (20) structure shown in Fig. 1 is only a slightly less stable local minimum, with $D_e = 719\ cm^{-1}$ (Fig. 3a). It is characterized by an Ar dimer lying above the aromatic ring, with one Ar atom binding to the centre of the ring like in (10) at $R_e = 3.41$ Å and $x_e = 0.43$ Å and the second Ar ligand located at $R_e = 2.68$ Å above the five-membered H–C–C–O–H ring formed by the OH group. The Ar–Ar distance of 3.7 Å in (20) is close to one of the isolated Ar_2 dimers. In this (20) structure, Ar_2 can maximize the sum of the dispersion interaction with the aromatic ring and the induction interaction with the dipole of the OH group. Interestingly, the M06-2X energy gap between (20) and (11) of ~40 cm^{-1} is much smaller than the one predicted recently at the MP2 level (~250 cm^{-1}).[39] For completeness, it is noted that there are a variety of related (20)-type isomers, which are obtained from the most stable one shown in Fig. 1 by internal rotation of Ar_2 above the aromatic plane (see Fig. S1 in ESI‡). These are, however, ~70–120 cm^{-1} less stable than the most stable one and thus not considered further. The substantial barrier $V_b = 165\ cm^{-1}$ between the most stable (20) isomer and the lowest neighbouring local minimum occurs at a transition state with Ar above the O atom and prevents facile Ar_2 internal rotation under cold molecular beam conditions. Interestingly, there is a considerable less stable third type of isomer, namely (H10). Its dissociation energy of $D_e = 548\ cm^{-1}$ is close to the sum of those of (H00) and (10), $D_e = 540\ cm^{-1}$. The intermolecular H/π-bonds in (H10) are very similar to those of the corresponding (H00) and (10) dimers due to little interaction between the two Ar ligands, which are separated by a distance (6.4 Å) much larger than the Ar_2 equilibrium distance. Another identified solvation motif for $n = 2$ is denoted $(11)^H$ and involves nonlinear bifurcated H-bonding to both equivalent Ar atoms in a C_{2v} symmetric structure in which the OH group

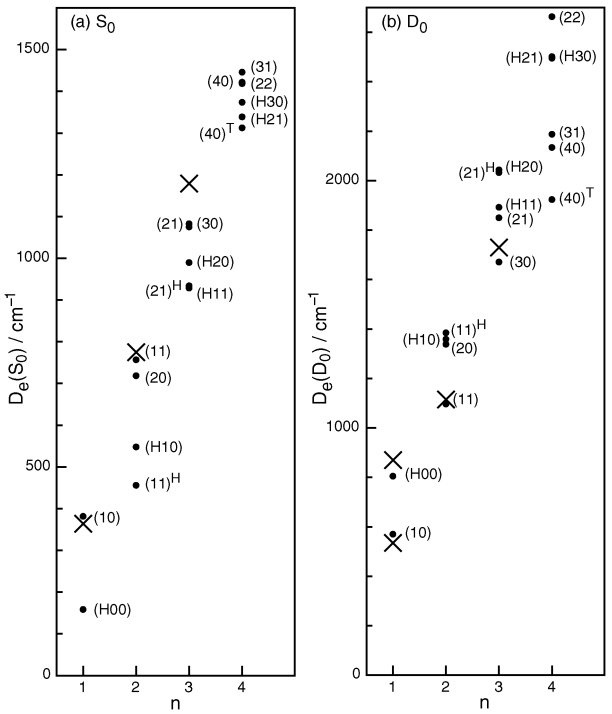

Fig. 3 Interaction energies (D_e in cm^{-1}) of various isomers of $PhOH^{(+)}$–Ar_n clusters ($n \leq 4$, Fig. 1) in the S_0 (a) and D_0 (b) states calculated at the M06-2X/aug-cc-pVTZ level. The crosses indicate available experimental binding energies (Table 2).

points toward the midpoint of an Ar_2 dimer in a T-shaped fashion. In the S_0 state, this isomer is however high in energy (D_e = 465 cm^{-1}).

The (30) isomer, in which a nearly symmetrical Ar_3 triangle is attached to the aromatic ring, is the most stable structure of PhOH–Ar_3 (Fig. 1). This structure is derived from the most stable (20) isomer by adding a third Ar ligand to the second available binding site near the OH group. The calculated interaction energy of 1083 cm^{-1} is compatible with the experimental estimate of 1179 ± 45 cm^{-1} (Table 2, Fig. 3a).[41] Again, there are several less stable (30)-type isomers, which can be obtained by internal rotation of the planar Ar_3 triangle above the aromatic plane. These are, however, less stable and not considered further because they are not detected experimentally. For example, the (30) isomer obtained by rotation of ~180° is 145 cm^{-1} higher in energy than the most stable (30) structure depicted in Fig. 1. Although the barriers for internal rotation in (30) were not calculated, they are probably larger than those between the various (20) minima of PhOH–Ar_2, because two rather than one Ar ligands have to overcome individual local barriers.

The most stable (21)-type isomer is only slightly less stable than the most stable (30) isomer, D_e = 1075 *vs.* 1083 cm^{-1}. Again, there are several less stable (21)-type rotamers, which differ from the one shown in Fig. 1 by the orientation of the Ar_2 unit with respect to the OH group. Similar to the n = 2 complexes, isomers with an H-bonded ligand are less stable for n = 3, with dissociation energies of 929, 990, and 934 cm^{-1} for (H11), (H20), and $(21)^H$. Interestingly, whereas (11) is more stable than (20), the reversed energetic order is observed for (H11) and (H20) because the latter structure benefits from an additional Ar–Ar contact.

At this point, it is important to realize that PhOH–Ar_3 prefers solvation on a single side, because (30) is more stable than (21). This observation is in contrast to PhOH–Ar_2, which prefers solvation on both sides, as (11) is more stable than (20). This switch in preferred solvation pattern from double-sided to single-sided complexation upon attachment of the third Ar ligand is due to the substantial energy gain through the two additional Ar–Ar interactions, which is larger than the loss in PhOH–Ar interaction energy upon moving one Ar atom from above the centre of the aromatic ring to the less favourable binding site near the OH group. The analysis of the $S_1 \leftarrow S_0$ REMPI spectra in Fig. 2 presented in Section 3.2 confirms this switching scenario.

As expected from the binding energies of the n = 3 isomers, the (31) structure shown in Fig. 1 is found to be the most stable n = 4 isomer, with D_e = 1446 cm^{-1}. The next stable classes of isomers are of the types (40), (22), (H30), and (H21) with D_e = 1422, 1419, 1374, and 1339 cm^{-1}, respectively. The most stable (40) isomer has a nearly planar Ar_4 route attached to the PhOH plane. It is obtained from the most stable (30) isomer by adding a fourth Ar ligand in such a way that it has two Ar–Ar bonds and direct contact to PhOH. There are two such isomers and one is shown in Fig. 1. The isomer with a tetrahedral Ar_4 subcluster denoted $(40)^T$ is less stable (D_e = 1313 cm^{-1}), because the additional Ar–Ar interaction of the fourth Ar ligand is less favourable than the PhOH–Ar contact above two CH bonds of PhOH. Interestingly, the relative stability of isomers with H-bound ligands increases as a function of cluster size, in particular for structures in which the H-bonded ligand has contact to out-of-plane Ar ligands attached above the ring. One such structure is the (H30) isomer shown in Fig. 1 with D_e = 1374 cm^{-1}, which is only 72 cm^{-1} less stable than the (31) global minimum.

In general, dispersion forces dominate the attraction in neutral PhOH–Ar_n clusters. As these forces are nearly additive, the binding energies of the various isomers can be approximated by pairwise addition of the respective Ar–Ar and PhOH–Ar interactions. Hence, the most stable isomers have then structures, which maximize these interactions under the constraints of steric hindrance and the anisotropy of the PhOH–Ar dimer potential. To illustrate the degree of additivity, we mention as an example the energy difference of (31) and (30), which is close to the binding energy of (10) (1446 − 1083 = 363 ≈ 382 cm^{-1}). This near additivity in the total binding energies leads to a preferential cluster growth in the order (10), (11), (30), and (31) for n = 1–4, respectively (Fig. 3). This sequence obtained for the D_e values at the M06-2X level exhibits alternation in single- and double-sided solvation in the small size regime considered (in line with the REMPI spectra in Fig. 2), although, interestingly, the energic order of the nearly isoenergetic (30) and (21) isomers is changed when considering the D_0 values at the M06-2X level (Table 2) or the MP2 level.[39] As a general trend, isomers with H-bound ligands will become more competitive for larger cluster sizes n because of the additional Ar–Ar interactions of the H-bonded ligand with further ligands above and below the ring (Fig. 3a). Thus, the energy gap between (H30) and (31) of 72 cm^{-1} is much smaller than the one between (30) and

(H11) of 154 cm^{-1} and the one between (10) and (H00) of 224 cm^{-1}. For the same reason, isomers with in-plane H-bonds of Ar ligands to CH protons of PhOH are expected to become more competitive in the size range beyond the one considered here ($n \leq 4$).[34] In general, the cluster growth predicted for PhOH–Ar_n by the M06-2X calculations is similar to the one postulated for the isoelectronic aniline–Ar_n clusters according to empirical potential calculations.[59,60] This suggested that cluster growth sequence is also consistent with the O–H stretching frequencies calculated for (10), (11), (30), and (31). The predicted complexation-induced redshifts of −2.3, −3.8, −6.4, and −9.6 cm^{-1} are systematically larger but compatible with the measured shifts of −2, −2, −4, and −5 cm^{-1}, respectively (Table S1 in ESI‡).[37]

3.2 S_1 state

The REMPI spectra of the $S_1 \leftarrow S_0$ transition of PhOH–Ar_n in Fig. 2 were recorded by two-color soft ionisation to avoid ionisation-induced fragmentation.[37] In general, these spectra are in good agreement with corresponding spectra reported previously.[27–29,31,33,38–40,61] The spectra are plotted with respect to $S_1 0^0$ of PhOH at 36 350 cm^{-1}. The positions of the S_1 origins identified are listed in Table 3, along with the suggested isomer assignment. The assignments for $S_1 0^0$ of (10) and (11) at −34 and −69 cm^{-1} were recently confirmed unambiguously by rotationally-resolved LIF spectroscopy.[29] The low rotational temperature derived from these spectra, $T_{rot} < 10$ K, suggests that also the vibrational temperature of the PhOH–Ar_n clusters is quite low, in line with the absence of any intermolecular hot bands in the REMPI spectra in Fig. 2. Thus, all bands in Fig. 2 are attributed to the intermolecular vibrational structure of isomers in S_1. Hole-burning reveals that the $n = 1$ and $n = 2$ spectra are dominated by a single isomer.[31] The $S_1 0^0$ assignments of (20), (21), (30), and (31) are mainly based on the empirical additivity model developed recently.[37] Thus, one of the central goals of the present work has been the confirmation of this tentative isomer assignment *via ab initio* methods. To this end, RI-CC2/aug-cc-pVDZ calculations are carried out, and S_1 excitation spectra are simulated using the FC approximation. The S_1 state calculations considered only the lower-energy isomers of PhOH–Ar_n, as identified by the M06-2X calculations in S_0. This strategy appears to be justified because of the modest geometrical changes upon S_1 excitation for these structures, as evidenced by the small S_1 shifts (<100 cm^{-1}) and the intense $S_1 0^0$ transitions in the REMPI spectra in Fig. 2. The RI-CC2/aug-cc-pVDZ level has been chosen, because it reliably reproduced electronic transition energies of a variety of aromatic molecules and at the same time is sufficiently efficient to afford the exploration of larger clusters.[55] For example, the S_1 origin of PhOH is calculated as 36 359 cm^{-1}, which coincides with the experimental value to within 10 cm^{-1}. This agreement confirms that the electronic S_1 excitation is adequately described by the RI-CC2/aug-cc-pVDZ approach.

The additivity model developed on the basis of the experimental data states that the sequential attachment of the first, second, and third π-bonded Ar atoms on the same side of the aromatic ring induces incremental ΔS_1 shifts of −34, +32, and +25 cm^{-1}, respectively.[37] As the Ar ligands located on opposite sides of the ring do essentially not interact with each other, the total shift is simply the sum of the shifts induced by Ar ligands below and above the ring.[26,60] The predictions of this model are −34, −68, −2, +23, −36, and −11 cm^{-1} for (10), (11), (20), (30), (21), and (31), which agree with the experimental S_1 origins to within ±1 cm^{-1} (Table 3, Fig. 4a).[37] Thus, three parameters are sufficient to predict the S_1 origins of six isomers to within the experimental error. Within this new model, two new weak S_1 origins were

Table 3 ΔS_1 and ΔIP shifts (in cm^{-1}) calculated for various PhOH–Ar_n isomers compared to available experimental values and values derived from the additivity models

n	Isomer	ΔS_1 RI-CC2	ΔS_1 RI-CC2 additivity[c]	ΔS_1 Exp[a]	ΔS_1 Exp additivity[d]	ΔIP M06-2X	ΔIP Exp[b]
0		0 (36359)	0	0 (36350)	0	0 (68426)	0 (68628)
1	(H00)	−54				−675	
	(10)	−69	−69	−34	−34	−175	−176
2	(H10)					−802	
	(20)	−25	−25	−2	−2	−632	
	(11)	−148	−138	−69	−68	−421	−340
	$(11)^H$					−918	
3	(H20)					−982	
	(H11)					−960	
	(30)	+20	+20	+23	+23	−579	−551
	(21)	−104	−94	−37	−36	−770	
	$(21)^H$					−1049	
4	(H30)					−1071	
	(H21)					−1150	
	(40)	−7	−7			−762	
	$(40)^T$					−546	
	(31)	−67	−49	−12	−11	−820	−680
	(22)	−98[e]	−50[e]			−1130	

[a] Ref. 37. [b] Ref. 39–41, 43, 46, 63 and 66, assuming the isomer assignment from ref. 37. [c] Based on incremental shifts of −69, +44, +45, and −27 cm^{-1} for single-sided Ar solvation in the $n = 1$–4 complexes. [d] Based on incremental shifts of −34, +32, and +25 cm^{-1} for single-sided Ar solvation in the $n = 1$–3 complexes. [e] The strong deviation of the RI-CC2 calculated shift from that predicted by the additivity model is tentatively ascribed to cooperative interactions between the two Ar ligands which are close to the OH group.

identified in the REMPI spectra, namely the ones of (20) and (21).[37] Moreover, the structure of four isomers were tentatively assigned, namely (20), (21), (30), and (31).[37]

Fig. 4b visualizes the ΔS_1 shifts of PhOH–Ar$_n$ as obtained from the RI-CC2 calculations (Table 3). Only the most stable π-bonded (*km*) isomers determined at the M06-2X level in S_0 are considered. The derived pattern agrees well with the experimental one in Fig. 4a and fully confirms the isomer assignments derived from the empirical additivity model. In the following, we discuss the assignments of the S_1 origins in more detail for each cluster size. At this stage, it is important to realize that the ΔS_1 shifts upon Ar complexation directly reflect the change in the intermolecular binding energy upon electronic excitation.

The $n = 1$ REMPI spectrum is generated by a single isomer, namely (10), as proven by hole-burning and rotationally-resolved

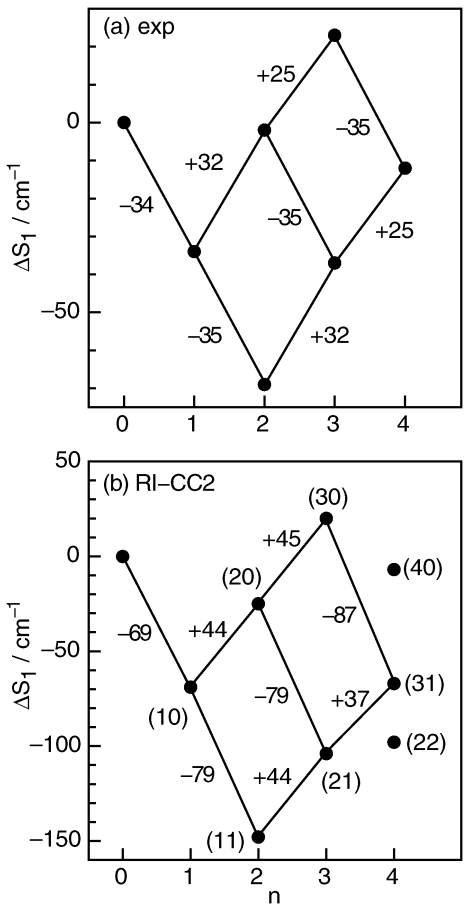

Fig. 4 (a) Experimental ΔS_1 shifts of various isomers of PhOH–Ar$_n$ ($n \leq 4$) with respect to the S_1 origin of bare PhOH ($n = 0$) at 36 350 cm^{-1}. These band origins can be reproduced to within ±1 cm^{-1} by an additivity model assuming incremental ΔS_1 shifts of −34, +32, and +25 cm^{-1} for the sequential attachment of the first, second, and third π-bonded Ar atoms on the same side of the aromatic ring. (b) ΔS_1 shifts calculated for various isomers of PhOH–Ar$_n$ ($n \leq 4$) with respect to the S_1 origin of bare PhOH ($n = 0$) at 36 359 cm^{-1}. These calculated band origins can be reproduced to within ±18 cm^{-1} by an additivity model assuming incremental ΔS_1 shifts of −69, +44, and +45 cm^{-1} for the sequential attachment of the first, second, and third π-bonded Ar atoms on the same side of the aromatic ring.

LIF spectroscopy.[29,31] The measured redshift of $\Delta S_1 = -34$ cm^{-1} is typical for π-bonding of Ar to aromatic molecules.[7] The ΔS_1 shift for (10) at RI-CC2/aug-cc-pVDZ is twice larger (−69 cm^{-1}), indicating that this level overestimates the Ar stacking interaction. Indeed, the (10) binding energy in S_0 determined at the RI-CC2 level ($D_0 = 623$ cm^{-1}) is almost twice as large as the experimental and M06-2X values (364 and 317 cm^{-1}). A similar observation was previously noted for the related π-bonded benzaldehydeH$^+$–Ar dimer, for which RI-CC2/aug-cc-pVDZ also overestimated the measured ΔS_1 redshift by a similar amount (−98 *vs.* −58 cm^{-1}).[55] Part of this overestimation is due to the neglect of BSSE in the RI-CC2 calculations. Test calculations reveal that correction for BSSE reduces the RI-CC2 binding energy of the (10) isomer of PhOH–Ar from 623 to 394 cm^{-1}. The predicted changes in the rotational constants of (10) upon S_1 excitation ($\Delta A_e = -36$ MHz, $\Delta B_e = 39$ MHz, $\Delta C_e = 37$ MHz) are consistent with the experimental values ($\Delta A_0 = -44$ MHz, $\Delta B_0 = 24$ MHz, $\Delta C_0 = 23$ MHz).[29] The major structural changes are a slight contraction of the Ar-ring separation ($\Delta R_e = 0.09$ Å) and a slight displacement toward the OH group ($\Delta x_e = 0.08$ Å), in line with previous conclusions.[34]

For comparison, we attempted also to determine ΔS_1 for the H-bonded PhOH–Ar structure. However, whereas (H00) is a local minimum in S_0 at both the RI-CC2 and the M06-2X levels, it is calculated to be a transition state for interconversion between the two equivalent π-bonded (10) global minima in S_1. The adiabatic transition for (H00) is predicted at $\Delta S_1 = -54$ cm^{-1}, *i.e.* between the S_1 origins of PhOH and (10). Interestingly, the barrier for π → H → π interconversion in S_1 of PhOH–Ar is slightly higher than in S_0 (by 15 cm^{-1}), although the OH group is slightly more acidic in S_1 leading to a stronger H-bond. However, the stabilisation of the π-bond upon S_1 excitation due to enhanced dispersion is even larger and overrides the stabilising effects on the H-bond.

The $n = 2$ REMPI spectrum is dominated by the (11) isomer, and the measured ΔS_1 shift of −69 cm^{-1} for the intense S_1 origin is twice that for (10), as expected for two equivalent Ar ligands attached to opposite sides of the PhOH ring. This structure is also proven by rotationally-resolved LIF spectroscopy.[29] The calculated ΔS_1 shift of −148 cm^{-1} is also roughly twice the shift predicted for the (10) dimer (−138 cm^{-1}) but again roughly twice the shift measured for (11) due to overestimation of the stacking interaction. The predicted changes in the rotational constants of (11) upon S_1 excitation ($\Delta A_e = -24$ MHz, $\Delta B_e = 22$ MHz, $\Delta C_e = 21$ MHz) are consistent with the experimental values ($\Delta A_0 = -18$ MHz, $\Delta B_0 = 12$ MHz, $\Delta C_0 = 13$ MHz).[29]

Although hole-burning experiments show that most of the structure in the REMPI spectrum is due to a single isomer, namely (11), the weak feature at $\Delta S_1 = -2$ cm^{-1} has recently been suggested as $S_1 0^0$ of the less stable (20) isomer on the basis of the empirical additivity model.[37] The relative intensity of this band varies significantly with the expansion conditions in different experiments,[28,29,31,37,39,40,43,62] supporting its assignment to a less stable isomer. The calculated blueshift of +44 cm^{-1} with respect to (10) is in accord with the experimental value of +32 cm^{-1}. The same incremental blueshift was measured for (20) of isoelectronic aniline–Ar$_2$

(+32 cm^{-1}).[60] The intensity ratio for $S_1 0^0$ of (11) and (20) in the spectrum in Fig. 2 is ~10 and confirms the theoretical prediction that the binding energy of (11) is larger (by ~30–40 cm^{-1}) than that of (20). Assuming similar ionisation efficiencies for both isomers and the calculated ratios for the oscillator strengths (0.0233/0.0229) and the FC factors (0.71/0.33), the $S_1 0^0$ intensity ratio of ~10/1 observed in Fig. 2 yields a population ratio of 4.6/1 for (11)/(20). There are several less stable (20)-type isomers, which are obtained from the most stable (20) structure in Fig. 1 by internal rotation of the Ar_2 unit. However, the REMPI spectrum does not show any evidence for their population in the molecular beam. Significantly, their calculated S_1 origins differ quantitatively from that of the most stable (20) isomer so that we are confident that the one shown in Fig. 1 gives rise to the experimental signal. For example, $\Delta S_1 = -25$ and -42 cm^{-1} for the two lowest-energy (20) isomers. At this stage, we note that the predicted energy gap between (11) and (20) at M06-2X is much smaller than at MP2[39] (~30 *vs.* ~250 cm^{-1}). It is, however, difficult to judge from the experimental population ratio which energy difference is more reliable. Assuming thermodynamic equilibrium, the observed population ratio corresponds to effective temperatures of $T_{eff} = 28$ and 236 K using the M06-2X and MP2 energy gaps, respectively. From this consideration, the M06-2X energy gap appears to be more reasonable, because in this case T_{eff} would be closer to the rotational temperature of $T_{rot} \approx 5$ K.[29] It would be quite useful to confirm the (20) geometry by LIF spectroscopy of the $\Delta S_1 = -2$ cm^{-1} band at rotational resolution.[29] The predicted rotational constants for (20) are $A_e = 1145$, $B_e = 675$, and $C_e = 538$ MHz, with changes upon S_1 excitation of $\Delta A_e = +80$, $\Delta B_e = -54$, and $\Delta C_e = -17$ MHz. These parameters are quite different from those of the (11) isomer.

According to the empirical additivity model, the intense $S_1 0^0$ band with $\Delta S_1 = +23$ cm^{-1} in the $n = 3$ REMPI spectrum was recently assigned to (30), whereas the weak origin with $\Delta S_1 = -37$ cm^{-1} was newly identified as (21).[37] Indeed, the M06-2X calculations show that (30) is slightly more stable than (21), although the energetic order changes when harmonic ZPE corrections are taken into account. Moreover, the calculated incremental ΔS_1 shifts of +45 cm^{-1} for (20) → (30) and +44 cm^{-1} for (11) → (21) are consistent with the corresponding experimental values of +25 and +32 cm^{-1} and fully support this scenario (see Fig. 4). The hole-burning spectrum of the $n = 3$ complex is also compatible with the existence of these two isomers,[31] because burning of the intense $S_1 0^0$ band of (30) did not affect the weak signals attributed to (21).[37] PIE and fragmentation spectra from the $\Delta S_1 = +23$ cm^{-1} origin also confirm that this band is from an isomer with only π-bonded ligands, although the exact position of the Ar ligands could not be determined.[41] The same conclusion was derived from time-resolved IR spectra of the $n = 3$ cation prepared by REMPI *via* the $\Delta S_1 = +23$ cm^{-1} origin, which convincingly show that π → H isomerisation of one of the three π-bonded Ar ligands occurs after ionisation.[37] Assuming similar ionisation efficiencies for both isomers and the calculated ratios for the electronic transition dipole moments (0.0238/0.0229) and the FC factors (0.033/0.020), the $S_1 0^0$ intensity ratio of ~11/1 in Fig. 2 yields a population ratio of 6.4/1 for (30)/(21). Assuming $T_{eff} = 10$ K, this population ratio translates into an energy gap of 13 cm^{-1} in favour of (30). This value is compatible with the difference in the M06-2X interaction energies of 8 cm^{-1} but seems to be in conflict with the MP2 prediction that (21) is about 110 cm^{-1} more stable than (30).[39] As also the RI-CC2 level predicts the (21) structure to be more stable than (30) one may conclude that these correlated levels overestimate dispersion and thus π-bonding to the centre of the ring relative to other binding sites, leading to a strong preference for double-sided solvation in neutral PhOH–Ar_n clusters in the small size regime. As for (10) and (11),[29] rotationally-resolved LIF spectra would be definitive in assigning the geometric structures responsible for the $\Delta S_1 = +23$ and -37 cm^{-1} origins of $n = 3$. The predicted rotational constants are $A_e = 680$, $B_e = 488$, and $C_e = 474$ MHz for (30), which are rather different from those of (21), $A_e = 866$, $B_e = 371$, and $C_e = 299$ MHz.

At this stage it is interesting to note that the $n = 2$ population in the molecular beam is dominated by the (11) isomer, whereas the $n = 3$ population is mainly due to (30). Although this result is consistent with the thermodynamic results of the present M06-2X calculations, the nearly quantitative switch from preferential double-sided to single-sided solvation is striking, and at first glance difficult to rationalize assuming a cluster growth by sequential ligand attachment, *i.e.* (10) → (11) → (21). In fact, the latter argument has motivated a preferential assignment to (21) rather than (30).[40,42] However, due to the high-collision rate in the initial stage of the molecular beam expansion, frequent ligand exchange reactions during the three-body collisions required for cluster growth are readily able to induce a growth sequence involving (10) → (11) → (21) followed by Ar + (21) → (30) + Ar ligand exchange, in order to produce the thermodynamically most stable $n = 3$ complex.

The empirical additivity model suggests an assignment of $S_1 0^0$ with $\Delta S_1 = -12$ cm^{-1} in the $n = 4$ REMPI spectrum to (31), which is indeed the most stable isomer in S_0 obtained by the M06-2X calculations. This assignment is fully supported by the comparison of the experimental and calculated ΔS_1 shift patterns in Fig. 4, which are very much in favour of (31) rather than the less stable (40) and (22) isomers. The calculated incremental ΔS_1 shift of +37 cm^{-1} for (21) → (31) is compatible with the measured shift of +35 cm^{-1}. We note that our current assignment to (31) revises the recent interpretation as (40).[39,43] The (40) assignment is not only in conflict with the MP2[39] and M06-2X interaction energies but also with the ΔS_1 additivity pattern in Fig. 4.

The comparison of the FC simulations with the experimental REMPI spectra in Fig. 5 provides further support for the given isomer assignments. In this figure, the calculated S_1 origins of the various isomers are shifted to match the experimental S_1 origins. Moreover, the frequency scale of all calculated spectra is compressed by a single unique factor of 0.752 to account for the large anharmonicity of the intermolecular modes. As mentioned in Section 3.1, a scaling factor of ~0.7 is derived from comparison between harmonic and anharmonic frequencies of (10) in S_0. As can be seen from Fig. 5, there is semi-quantitative agreement between the experimental and simulated spectra with respect to relative

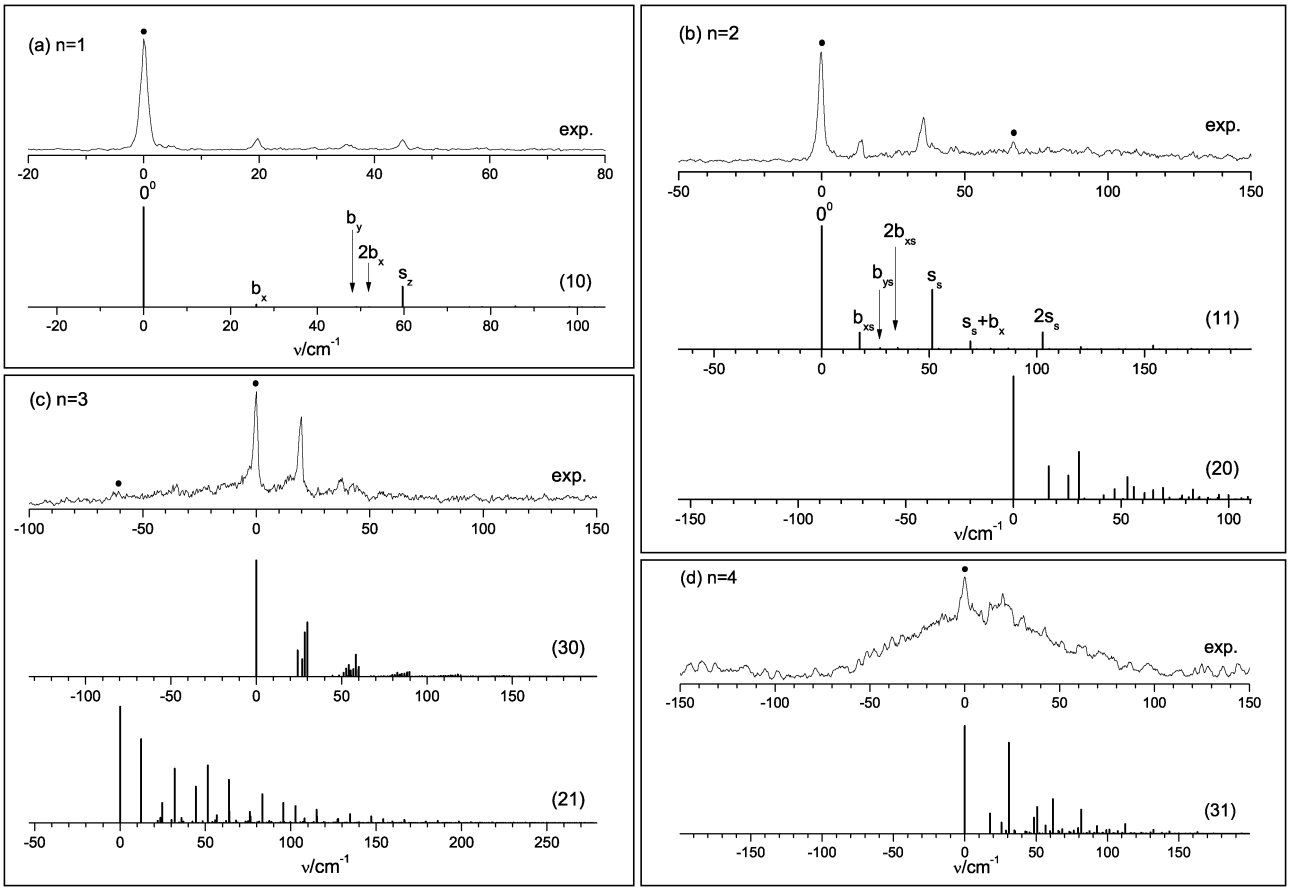

Fig. 5 Harmonic Franck–Condon simulations of the $S_1 \leftarrow S_0$ transitions of various isomers of PhOH–Ar$_n$ with n = 1–4 (Fig. 1) at the RI-CC2/aug-cc-pVDZ level compared to experimental spectra (Fig. 2). The frequency scale of all calculated spectra is compressed by a factor of 0.752 and shifted to match experimental and calculated S_1 origins. Experimental S_1 origins are indicated by filled circles (Table 3). Vibrational assignments of intermolecular modes indicated for (10) and (11) are listed in Table S2 in ESI.‡

positions and intensities, which provides further confidence of the given isomer assignment and also suggestions for the vibrational mode assignment. The vibrational assignments for the intermolecular modes of (10) and (11) are included in Fig. 5 with the notation adapted from ref. 62. For details of this assignment we refer to ref. 31, 34, 40 and 62 and Table S2 in ESI.‡ The normal modes of all other isomers involve Ar subcluster internal vibrations and thus are more complex. A detailed analysis of these modes is clearly beyond the scope of the present work.

In summary, the RI-CC2 calculations for the $S_1 \leftarrow S_0$ transition of PhOH–Ar$_n$ provide a convincing assignment of the S_1 origins observed in experimental REMPI spectra to the corresponding structural isomers by reproducing the additivity rule established empirically (Fig. 4, Table 3). Experimentally, the sequential attachment of the first, second, and third π-bonded Ar atoms on the same side of the aromatic ring induces incremental ΔS_1 shifts of −34, +32, and +25 cm^{-1},[37] while the corresponding RI-CC2 values are −69, +44, and +45 cm^{-1}, respectively. These calculated band origins can be reproduced to within ±18 cm^{-1} by the theoretical additivity model assuming incremental ΔS_1 shifts of −69, +44, and +45 cm^{-1} for the sequential attachment of the first, second, and third π-bonded Ar atoms on the same side of the aromatic ring. Overall, the crude RI-CC2/aug-cc-pVDZ approach provides a semi-quantitative picture of the transition frequencies of these weakly bound floppy molecules, and the degree of agreement with experiment is satisfactory considering the approximations involved in this scheme. These include the restrictions of the RI-CC2 model, the moderate size of the aug-cc-pVDZ basis set, and the assumption of harmonic zero-point corrections. The same conclusion holds for the FC simulations. Furthermore, it is noted that the ΔS_1 pattern is quite sensitive to the Ar binding sites and provides thus a much more solid criterion for isomer assignments than the delicate evaluation of quantum chemical binding energies for isomers with small energy differences. For example, although the relative energetic order established for various isomers sensitively depends on the way ZPE is accounted for, the ΔS_1 pattern and resulting additivity pattern are quite robust against ZPE corrections (Fig. 5 and Fig. S2 in ESI‡), because ΔS_1 shifts result from energy differences in two different states and thus large ZPE effects may readily cancel.

In an effort to rationalize the direction of the incremental ΔS_1 shifts, the π (HOMO) and π* (LUMO) orbitals involved in $S_1 \leftarrow S_0$ excitation of PhOH are considered in Fig. 6. S_1 excitation reduces the electron density in the centre above the aromatic ring and allows for a closer approach of the

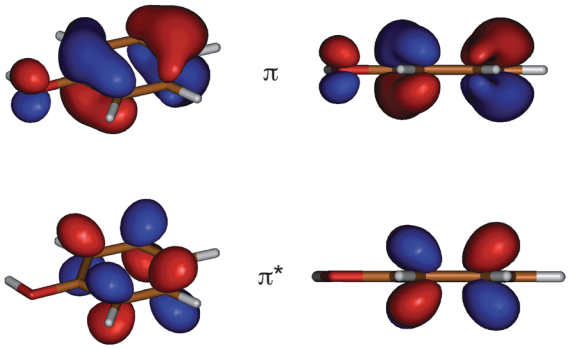

Fig. 6 HOMO (π) and LUMO (π*) orbitals of PhOH involved in $S_1 \leftarrow S_0$ excitation of PhOH–Ar$_n$ clusters derived from RI-CC2/aug-cc-pVDZ calculations.

Ar ligand in (10) and (11) due to reduced Pauli repulsion. At the same time, the extended π electron density increases its polarisability and the resulting dispersion attraction. Both effects increase the binding energy of PhOH–Ar in the (10) configuration upon S_1 excitation leading to an S_1 redshift. On the other hand, the second and third Ar ligands in (20) and (30) attached above the OH moiety experience enhanced Pauli repulsion in S_1 due to higher π electron density in this region, and the reduced interaction induces incremental S_1 blueshifts.

3.3 D_0 state

Optimised equilibrium structures of various isomers of PhOH$^+$–Ar$_n$ in the D_0 state obtained at the M06-2X/aug-cc-pVTZ level are shown in Fig. 1, and the total stabilisation energies are listed in Table 2 and visualized in Fig. 3b. The agreement between the binding energies calculated for the H-bonded (H00) and π-bonded (10) isomers of PhOH$^+$–Ar and the measured dissociation energies confirms the suitability of this approach for a reliable description of both interaction motifs for the PhOH$^+$–Ar cation.

The planar H-bound (H00) structure with C_s symmetry corresponds to the global minimum of the PhOH$^+$–Ar potential, as induction forces provide a major contribution to the attraction. The nearly linear H-bond is about four times stronger than that for neutral PhOH–Ar and characterized by D_e = 805 cm^{-1}, R_{H-Ar} = 2.35 Å, θ_{O-H-Ar} = 178.6°, and an intermolecular stretch frequency of 85 cm^{-1}. The calculated binding energy is in the range of recent experimental values estimated from PIE and MATI studies of PhOH$^+$–Ar$_n$ with n = 2 and 3 ($D_0 \approx$ 870 and ~905 cm^{-1}).[41,46] These values are probably more reliable than the earlier estimate of 650 ± 150 cm^{-1} based on the analysis of IRPD spectroscopy of PhOH$^+$–Ar$_n$ clusters.[13]

The π-bonded (10) local minimum is significantly less stable than (H00). The calculated interaction energy of 571 cm^{-1} agrees well with the measured binding energy of 535 ± 3 cm^{-1}.[47] Ionisation increases the interaction strength by 189 cm^{-1} (~50%), leading to a contraction of the Ar-ring separation from 3.40 to 3.28 Å and an increase in the intermolecular stretch frequency from 63 to 78 cm^{-1}. Moreover, the Ar atom is much more displaced from the centre of the aromatic ring toward the OH group in the D_0 state (x_e = 1.24 Å) as compared to S_0 and S_1, consistent with the extended FC progression of the corresponding b_x bending mode in the photoelectron spectra.[40] In fact, the Ar atom in (10) is interacting closely with the C1 atom of the COH unit, in line with high level *ab initio* calculations.[45] The harmonic intermolecular frequencies of 33, 50, and 78 cm^{-1} are larger than the experimentally assigned fundamental frequencies of 15, 25, and 66 cm^{-1},[40] mainly due to anharmonicity effects, which are larger for the bending than the stretching modes.

The ionisation-induced π → H switch in the preferred PhOH–Ar interaction motif as well as the ionisation-induced structural changes in the geometry of the (10) isomer may be rationalized by analysing the atomic charge distributions of PhOH and PhOH$^+$ shown in Fig. 7, which result from the natural bond orbital (NBO) analysis at the M06-2X level. Ionisation increases the positive partial charge on the C1 atom of the COH group, which explains the substantial shift of Ar from the centre of the ring toward C1 upon ionisation of (10) and the concurrent increase in the interaction energy. The cation features also high positive partial charge on the five-membered H–C–C–O–H ring (+0.49 e) leading to strong attraction of Ar atoms located above this ring. Also the OH proton carries high positive partial charge in PhOH$^+$, leading

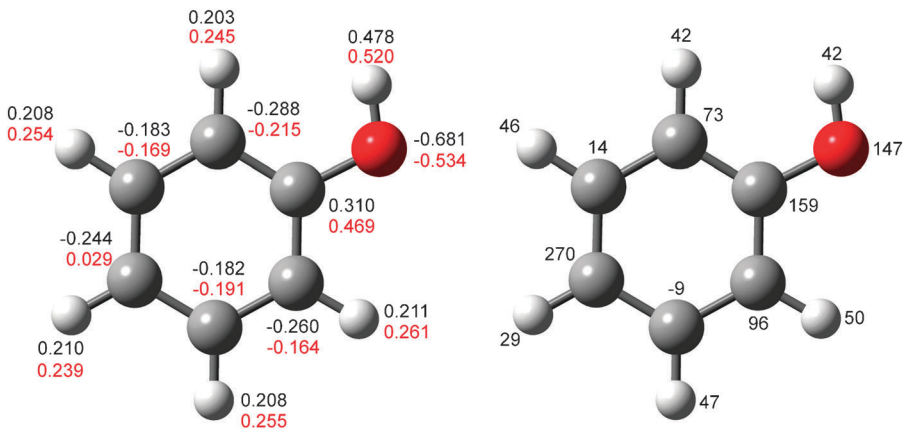

Fig. 7 (left) NBO atomic charges (in units of e) for PhOH and PhOH$^+$ in the S_0 (top) and D_0 (bottom) states evaluated at the M06-2X/aug-cc-pVTZ level. (right) Difference in NBO charges (in units of 0.001 e) of PhOH in the ionic and neutral ground state, $\Delta q = q(D_0) - q(S_0)$.

to substantial stabilisation of the H-bond of (H00) in the D_0 state.

The interaction energies calculated for the two most stable $n = 2$ isomers $(11)^H$ and (H10) shown in Fig. 1 are quite similar, $D_e = 1384$ and 1359 cm^{-1}. The energetic order is in fact reversed when ZPE is taken into account, $D_0 = 1175$ and 1217 cm^{-1}. The (H10) isomer features a nearly linear H-bonded Ar ligand and a π-bonded ligand above C1. As the two intermolecular bonds are similar to those in (H00) and (10), the total interaction energy in (H10) is nearly the sum of the two individual bond energies. In the $(11)^H$ isomer with C_s symmetry, the acidic OH proton binds to the centre of the Ar_2 bond in a perpendicular fashion, leading to a bifurcated binding motif with two highly nonlinear O–H–Ar bonds ($R_{H-Ar} = 2.57$ Å, $\theta_{O-H-Ar} = 134.7°$). These are substantially longer than the nearly linear H-bond in (H00). Nonetheless, the $(11)^H$ structure is significantly stabilised by the interaction of both Ar ligands with the nearby high positive partial charge of the OH proton. While this isomer is high in energy for neutral PhOH–Ar_2, it becomes competitive in energy with the strongly bound (H00) cluster in the ionic D_0 state. Also the most stable (20)-type isomer of the cation with $D_e = 1338$ cm^{-1} is quite low in energy. It has the same Ar_2 orientation as in the S_0 state and other (20) isomers are less stable by at least 300 cm^{-1} (Fig. S3 in ESI‡). Moreover, the barriers for internal rotation of the Ar_2 unit are much higher in the ionic cluster. For example, the barrier amounts to $V_b = 527$ cm^{-1} for internal rotation toward the neighbouring local minimum *via* a transition state with Ar above the O atom. The (20) cation is also stabilised by the strong attraction of the second Ar ligand with the nearby proton. When compared to (H10), the loss in energy in (20) induced by the large deviation of the H-bond to the first Ar ligand from linearity is largely compensated for by gain through the additional Ar–Ar contact. The considerably less stable (11) isomer of $PhOH^+$–Ar_2 is observed by REMPI of neutral (11), and its measured dissociation energy of $D_0 \approx 1115$ cm^{-1} is close to the predicted value ($D_e = 1097$ cm^{-1}). The latter one is slightly less than twice the (10) binding energy (571 cm^{-1}), indicating that the equivalent intermolecular π-bonds in (11) are slightly weaker and longer (by 0.02 Å) than those in (10).

The predicted interaction energies for the two most stable $n = 3$ isomers (H20) and $(21)^H$ are almost identical, $D_e = 2043$ and 2033 cm^{-1}, and the energetic order is again reversed when ZPE is taken into account, $D_0 = 1697$ and 1726 cm^{-1}. These structures have two Ar ligands close to the OH proton and thus are significantly more stable than (H11) with $D_e = 1893$ cm^{-1}. The latter value is close to the sum of the (H00) and (11) binding energies (1902 cm^{-1}), consistent with the small interaction between the π-bonded and H-bonded Ar ligands in (H11). Even higher in energy are the (30) and (21) isomers because they feature only π-bonded ligands. The (30) isomer is observed in the REMPI experiments, and its calculated dissociation energy (1671 cm^{-1}) is close to the measured value (1730 ± 30 cm^{-1}).[41] As the (21) minimum is quite flat, no real minimum could be localized, probably due to a very low barrier for isomerization toward (H11).

The most stable $PhOH^+$–Ar_4 isomer is (22) with $D_e = 2663$ cm^{-1} (C_s symmetry), followed by (H30) and (H21) with $D_e = 2502$ and 2495 cm^{-1}, respectively. As the (H21) minimum is quite flat, no real minimum could be localized, probably due to a very low barrier for isomerization toward (22). All these $n = 4$ isomers feature strong interactions with the OH proton. The (31) isomer observed in the REMPI experiments is significantly less stable with $D_e = 2187$ cm^{-1}. Even higher in energy are (40) and $(40)^T$ featuring single-sided ring solvation without strong Ar interactions with the OH proton.

The adiabatic ionisation potentials for the various PhOH–Ar_n isomers are compared to available experimental values in Table 3 and Fig. 8. Similar to ΔS_1, the ΔIP shifts induced by Ar complexation directly reflect the change in the intermolecular interaction energy upon ionisation. The experimental IP of PhOH (68 628 cm^{-1})[63] is well reproduced (to within 0.3%) by the M06-2X calculations (68 426 cm^{-1}), indicating that this level is adequate to describe the ionisation process of the bare aromatic molecule by removal of the π electron from the HOMO.

The ΔIP shift predicted for (10) matches the measured value of −176 cm^{-1} and reflects the substantial increase in π-interaction upon ionisation due to additional charge-induced dipole attraction (by ∼50%). In contrast, the predicted ΔIP for (H00) is much larger (−675 cm^{-1}), indicative of the strong intermolecular H-bond in the D_0 state. As expected from ΔS_1, the ΔIP shifts for (11) and (H10) are nearly additive,

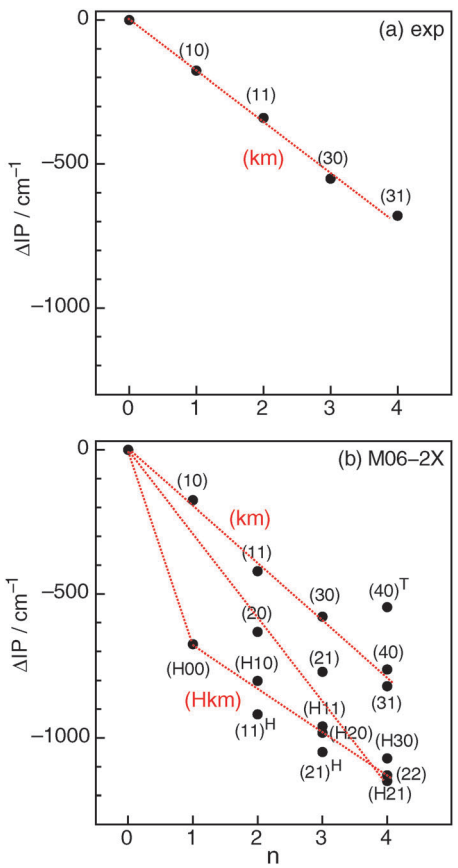

Fig. 8 (a) Experimental ΔIP shifts of various isomers of PhOH–Ar_n ($n \leq 4$) with respect to the IP of bare PhOH ($n = 0$) at 68 628 cm^{-1}. (b) ΔIP shifts calculated for various isomers of PhOH–Ar_n ($n \leq 4$) with respect to the IP of bare PhOH ($n = 0$) at 68 426 cm^{-1}.

and the shift predicted for (11) is compatible with the measured shift (−421 *vs.* −340 cm^{-1}). Interestingly, ΔIP for (20) is significantly larger than for the (11) isomer (−632 *vs.* −421 cm^{-1}). This result is in line with the fact that (20) is more stable than (11) in the D_0 state, whereas the energetic order is reversed in S_0. Thus, (20) is largely stabilised upon ionisation by the strong interaction of the second Ar ligand with the nearby OH proton (Fig. 1). Interestingly, the stabilisation of $(11)^H$ upon ionisation is largest of all $n = 2$ isomers investigated, namely ΔIP = −918 cm^{-1}, because two Ar ligands are close to the nearby proton.

In contrast to the ΔS_1 shifts, the experimental ΔIP shifts are less sensitive to the exact location of the π-bonded ligands. This trend can be extracted from the measured and calculated ΔIP plots in Fig. 8a and b, which show a nearly linear dependence as a function of *n*. This observation indicates that the additional charge-induced dipole attraction in the D_0 state is relatively insensitive to the Ar position above the aromatic ring. This result is true for isomers with and without H-bound ligands, (H*km*) and (*km*). The slope is slightly smaller for (H*km*) than for (*km*), a typical effect observed for interior ion solvation by surrounding inert ligands.[4,48,64,65] The measured slope for (*km*) of −174 cm^{-1} per ligand agrees well with the calculated one of −201 cm^{-1} per ligand. In particular, the predicted ΔIP shifts for (30) and (31), −579 and −820 cm^{-1}, are consistent with the measured values of −551 and −680 cm^{-1}, supporting the given isomer assignments. The slope of ∼150 cm^{-1} per π-bonded ligand along the (H*km*) series is 25 cm^{-1} smaller than the one for the (*km*) series owing to the above-mentioned noncooperative nonadditive effects of the induction forces for interior ion solvation. As a rough rule, addition of a π-bonded ligand above the ring reduces the calculated IP by 200 cm^{-1} in the size range considered ($n \leq 4$), whereas an additional H-bonded Ar ligand reduces it by 500–700 cm^{-1}. While this trend for π-bonded ligands is confirmed by the experimental data for (*km*) isomers of PhOH–Ar_n, no directly measured value exists for ΔIP of any (H*km*) isomer. The experimental value for ΔIP of (H00) can however be estimated from the difference of the binding energies of (H00) in the S_0 and D_0 states, according to $D_0(S_0) - \Delta IP = D_0(D_0)$. As $D_0(D_0)$ was measured as ∼870 cm^{-1},[41] and $D_0(S_0)$ must be smaller than the binding energy of (10) in S_0 (364 cm^{-1}), the experimental value for ΔIP of (H00) lies in the range between −870 and −506 cm^{-1}, leading to a value of −688 ± 182 cm^{-1} consistent with the prediction of −675 cm^{-1}. Inspection of Fig. 8b actually reveals that the slope resulting from ΔIP of (20) and (22) of −290 cm^{-1} per ligand is much larger than those of the (*km*) and (H*km*) series. This result is attributed to the large additional stabilising effect of the strong interaction of the Ar ligands with the nearby OH proton in the D_0 state of these isomers, which is however still smaller than that for a linearly H-bonded ligand. The predictions in Fig. 8b allow for the following conclusions. (1) Comparison with Fig. 8a confirms the assignments for (10), (11), (30), and (31) developed from the additivity model for ΔS_1. (2) Predictions for the ΔIP shifts are provided for (20) and (21). These isomers are produced in the molecular beam and identified by weak S_1 origins in the REMPI spectra in Fig. 2. However, no photoionisation spectra have been reported yet, although the IP values extracted from such spectra would be valuable probes for their structural assignments.

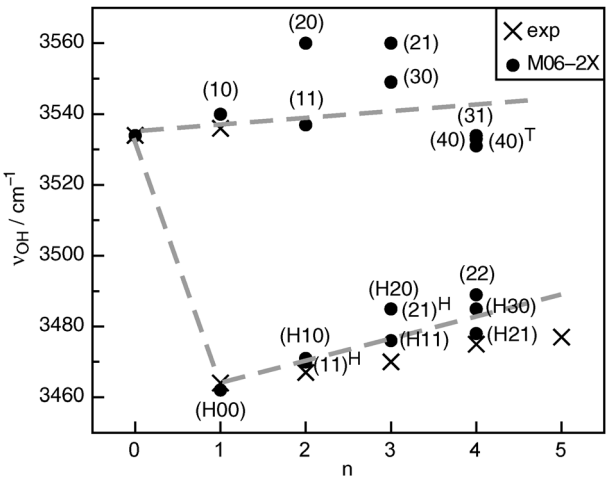

Fig. 9 O–H stretch frequencies (ν_{OH}) of the most stable isomers of $PhOH^+$–Ar_n calculated at the M06-2X/aug-cc-pVTZ level compared with the corresponding experimental values derived from IRPD spectra of clusters generated in the EI source (Table 4).[13] The widths of the experimental bands vary between 10 and 15 cm^{-1}.

Fig. 9 compares the O–H stretch frequencies (ν_{OH}) of the most stable isomers $PhOH^+$–Ar_n isomers calculated at the M06-2X level with the corresponding experimental values derived from IRPD spectra of clusters generated in the EI source (Table 4).[13] The widths of the experimental ν_{OH} bands are between 10 and 15 cm^{-1}, providing limits for the error bars on the fundamental frequencies. H-bonding induces a significant redshift (∼−70 cm^{-1}), whereas π-bonding causes small incremental blueshifts of a few cm^{-1}, and close agreement between experimental and calculated frequencies is observed. Interestingly, ν_{OH} of $(11)^H$ is similar to that of (H10),

Table 4 O–H stretch frequencies (ν_{OH} in cm^{-1}) of selected $PhOH^+$–Ar_n isomers calculated at the M06-2X level compared to available experimental values

n	Exp[a]	M06-2X	Isomer
0	3534	3534	
1	3463	3462	(H00)
	3536	3540	(10)
2	3467	3470	(H10)
		3471	$(11)^H$
		3537	(11)
		3560	(20)
3	3470	3476	(H11)
		3485	(H20)
		3485	$(21)^H$
		3549	(30)
		3560	(21)
4	3475	3485	(H30)
		3489	(22)
		3478	(H21)
		3531	(40)
		3533	$(40)^T$
		3534	(31)
5	3477		

[a] Ref. 13. The widths of the experimental bands vary between 10 and 15 cm^{-1}.

indicating that the $\Delta\nu_{OH}$ redshift induced by a single H-bonded ligand is similar to that induced by two bifurcated H-bonds to the two Ar ligands in $(11)^H$. As both $n = 2$ isomers have similar ν_{OH} frequencies and dissociation energies, they probably contribute to both the experimental IRPD spectra. The same conclusion holds for the $n = 3$ isomers (H20), (H11), and $(21)^H$ and also the corresponding $n = 4$ species. Thus the IRPD spectra are consistent with a cluster growth with two types of isomers in which an initial (H00) or $(11)^H$ cation cluster core is further solvated by π-bonded ligands.

The results of the current work enable us to suggest cluster structures involved in the previous ionisation, isomerisation, and fragmentation experiments of PhOH–Ar_n.[6,32,37,41,46,47,50,62] REMPI of neutral (10) generates (10) in the cationic state, which can subsequently isomerise toward the more stable (H00) isomer on the ps timescale (as was shown for $PhOH^+$–Kr)[50] and dissociate into $PhOH^+$ + Ar at the ionisation excess energy of $E_{exc} = 535 \pm 3$ cm^{-1}.[47] REMPI of neutral (11) produces (11) in the D_0 state, which undergoes isomerisation toward the more stable (H10) or $(11)^H$ isomers with a time constant of 7 ps.[6,32] This isomerisation process releases about ~300 cm^{-1} into intermolecular degrees of freedom and can then lead to dissociation into (H00) + Ar already at $E_{exc} \approx 200$ cm^{-1} or into $PhOH^+$ + 2Ar at $E_{exc} \approx 1115$ cm^{-1}.[46] REMPI of neutral (30) produces an ionic (30) cluster, which can isomerise quickly, for example, to (H20) on a timescale of less than 3 ps. This process releases also ~300–400 cm^{-1} internal energy into the cluster, which enables at $E_{exc} \approx 200$, ~900, and ~1700 cm^{-1} dissociation into (H10), (H00), and $PhOH^+$ by loss of one, two, and three Ar ligands, respectively.[41]

4. Concluding remarks

The structures and binding energies of neutral and ionic $PhOH^{(+)}$–Ar_n isomers with $n \leq 4$ have been investigated in the ground electronic states at the M06-2X/aug-cc-pVTZ level. This level was shown to reproduce the different types of intermolecular interactions present in these benchmark clusters to satisfactory accuracy. Dispersion forces dominate the attraction in neutral PhOH–Ar_n and thus π-bonding is more stable than H-bonding, leading to a preferred solvation sequence derived as (10), (11), (30), and (31) for $n \leq 4$, which is in line with the experimental REMPI and IR spectra. Significantly, the energy gap between clusters with and without H-bonded ligands decreases with increasing cluster size. The solvation sequence predicted recently at the MP2 level[39] is different from that at the M06-2X level and apparently not compatible with the experimental data, possibly due to overestimation of dispersion at the MP2 level. The $S_1 \leftarrow S_0$ excitation spectra of PhOH–Ar_n have successfully been interpreted with calculations at the RI-CC2/aug-cc-pVDZ level. These calculations fully confirm the isomer assignments by convincingly reproducing the pattern of the strongly isomer-dependent ΔS_1 origin shifts of the clusters and their intermolecular vibrational structure by means of FC simulations. The directions of the incremental ΔS_1 shifts are rationalized by the shape of the HOMO and LUMO orbitals of PhOH involved in $S_1 \leftarrow S_0$ excitation. Both H-bonding and the π-interaction slightly increase upon S_1 excitation, owing to the enhanced acidity of the OH group and increased polarisability of the aromatic π-electron system. In the $PhOH^+$–Ar_n cations, H-bonds are significantly stronger than π-bonds due to additional induction forces, leading to a π → H switch in the preferred interaction motif upon ionisation. Two competing solvation sequences are suggested by the M06-2X calculations, namely the formation of either a H-bonded (H00) dimer core or a $(11)^H$ trimer core, which are further solvated by π-bonded ligands in larger clusters. Both cluster growth sequences are compatible with the experimental IRPD spectra in the O–H stretch range. The predicted ΔIP shifts follow structural additivity rules, similar to the ones determined for ΔS_1. The consequences of the π → H switch triggered by ionisation on the isomerisation and fragmentation processes of $PhOH^{(+)}$–Ar_n are discussed in the light of the new structural and energetic cluster parameters.

The following future directions emerge from the present study. The isomer assignments for the S_1 origins of (20), (30), (21), and (31) may unambiguously be confirmed by rotationally-resolved LIF spectroscopy. Similarly, the ΔIP shifts predicted for (20) and (21) may be used to verify their structural assignments by photoionisation spectroscopy (*e.g.*, PIE, MATI). In addition, high-level calculations are desired to confirm the present identification of the interesting $(11)^H$ binding motif featuring two bifurcated OH–Ar hydrogen bonds as structural element in $PhOH^+$–Ar_n clusters, which can thermodynamically compete with the linear OH–Ar bond. The M06-2X/aug-cc-pVTZ level has been identified as efficient and promising model chemistry for scanning in detail the potential energy surfaces of small $PhOH^+$–Rg_n cation clusters, which are required as input for multi-dimensional FC simulations of the intermolecular vibrational structure observed in their photoionisation spectra as well as simulations of the dynamical isomerisation and fragmentation processes triggered by ionisation of this fundamental type of clusters. For example, both the energetics and dynamics of the π → H isomerisation process will strongly depend on the involved isomeric structure. To this end, the two $n = 2$ isomers (11) and (20) constitute simple systems to investigate in future these isomer-dependent dynamical processes at the molecular level.

Acknowledgements

This work was supported by the *Deutsche Forschungsgemeinschaft* (DO 729/4), a Grant-in-Aid for Scientific Research KAKENHI in the priority area 477 from MEXT (Japan), and the Core-to-Core Program of the Japan Society for Promotion of Science. M. S. is grateful for a fellowship from the Elsa Neumann foundation.

References

1 P. Hobza and K. Müller-Dethlefs, *Non-covalent interactions*, The Royal Society of Chemistry, Cambridge, 2010.
2 K. Müller-Dethlefs and P. Hobza, *Chem. Rev.*, 2000, **100**, 143.
3 C. E. H. Dessent and K. Müller-Dethlefs, *Chem. Rev.*, 2000, **100**, 3999.
4 O. Dopfer, *Z. Phys. Chem.*, 2005, **219**, 125.
5 B. Brutschy, *Chem. Rev.*, 2000, **100**, 3891.

6 S. Ishiuchi, M. Sakai, Y. Tsuchida, A. Takeda, Y. Kawashima, M. Fujii, O. Dopfer and K. Müller-Dethlefs, *Angew. Chem., Int. Ed.*, 2005, **44**, 6149.
7 X. Zhang and J. L. Knee, *Faraday Discuss.*, 1994, **97**, 299.
8 K. Müller-Dethlefs, O. Dopfer and T. G. Wright, *Chem. Rev.*, 1994, **94**, 1845.
9 T. Ebata, A. Fujii and N. Mikami, *Int. Rev. Phys. Chem.*, 1998, **17**, 331.
10 K. Kleinermanns, C. Janzen, D. Spangenberg and M. Gerhards, *J. Phys. Chem. A*, 1999, **103**, 5232.
11 N. Solcà and O. Dopfer, *Chem. Phys. Lett.*, 2001, **342**, 191.
12 N. Solcà and O. Dopfer, *Chem. Phys. Lett.*, 2000, **325**, 354.
13 N. Solcà and O. Dopfer, *J. Phys. Chem. A*, 2001, **105**, 5637.
14 N. Solcà and O. Dopfer, *J. Mol. Struct.*, 2001, **563/564**, 241.
15 N. Solcà and O. Dopfer, *Chem. Phys. Lett.*, 2003, **369**, 68.
16 A. Takeda, H. S. Andrei, M. Miyazaki, S. I. Ishiuchi, M. Sakai, M. Fujii and O. Dopfer, *Chem. Phys. Lett.*, 2007, **443**, 227.
17 A. Patzer, H. Knorke, J. Langer and O. Dopfer, *Chem. Phys. Lett.*, 2008, **457**, 298.
18 N. Solcà and O. Dopfer, *J. Chem. Phys.*, 2004, **120**, 10470.
19 A. Patzer, J. Langer, H. Knorke, H. Neitsch, O. Dopfer, M. Miyazaki, K. Hattori, A. Takeda, S. I. Ishiuchi and M. Fujii, *Chem. Phys. Lett.*, 2009, **474**, 7.
20 H. S. Andrei, N. Solca and O. Dopfer, *Phys. Chem. Chem. Phys.*, 2004, **6**, 3801.
21 N. Solcà and O. Dopfer, *Eur. Phys. J. D*, 2002, **20**, 469.
22 F. Pasker, N. Solcà and O. Dopfer, *J. Phys. Chem. A*, 2006, **110**, 12793.
23 Q. L. Gu and J. L. Knee, *J. Chem. Phys.*, 2008, **128**, 064311.
24 N. Solcà and O. Dopfer, *Phys. Chem. Chem. Phys.*, 2004, **6**, 2732.
25 H. S. Andrei, N. Solca and O. Dopfer, *J. Phys. Chem. A*, 2005, **109**, 3598.
26 N. Gonohe, H. Abe, N. Mikami and M. Ito, *J. Phys. Chem.*, 1985, **89**, 3642.
27 M. Mons, J. Le Calve, F. Piuzzi and I. Dimicoli, *J. Chem. Phys.*, 1990, **92**, 2155.
28 M. Schmidt, M. Mons and J. Le Calve, *Z. Phys. D: At., Mol. Clusters*, 1990, **17**, 153.
29 I. Kalkman, C. Brand, C. Vu, W. L. Meerts, Y. N. Svartsov, O. Dopfer, K. Müller-Dethlefs, S. Grimme and M. Schmitt, *J. Chem. Phys.*, 2009, **130**, 224303.
30 A. Fujii, M. Miyazaki, T. Ebata and N. Mikami, *J. Chem. Phys.*, 1999, **110**, 11125.
31 S. I. Ishiuchi, Y. Tsuchida, O. Dopfer, K. Müller-Dethlefs and M. Fujii, *J. Phys. Chem. A*, 2007, **111**, 7569.
32 S. I. Ishiuchi, M. Sakai, Y. Tsuchida, A. Takeda, Y. Kawashima, O. Dopfer, K. Müller-Dethlefs and M. Fujii, *J. Chem. Phys.*, 2007, **127**, 114307.
33 M. Ford, S. R. Haines, I. Pugliesi, C. E. H. Dessent and K. Müller-Dethlefs, *J. Electron Spectrosc. Relat. Phenom.*, 2000, **112**, 231.
34 J. Makarewicz, *J. Chem. Phys.*, 2006, **124**, 084310.
35 M. A. Vincent, I. H. Hillier, C. A. Morgado, N. A. Burton and X. Shan, *J. Chem. Phys.*, 2008, **128**, 044313.
36 J. Cerny, X. Tong, P. Hobza and K. Müller-Dethlefs, *J. Chem. Phys.*, 2008, **128**, 114319.
37 S. Ishiuchi, M. Miyazaki, M. Sakai, M. Fujii, M. Schmies and O. Dopfer, *Phys. Chem. Chem. Phys.*, 2011, **13**, 2409.
38 N. Gonohe, H. Abe, N. Mikami and M. Ito, *J. Phys. Chem.*, 1985, **89**, 3642.
39 A. Armentano, J. Cerny, M. Riese, M. Taherkhani, M. B. Yezzar and K. Müller-Dethlefs, *Phys. Chem. Chem. Phys.*, 2011, **13**, 6077.
40 S. R. Haines, C. E. H. Dessent and K. Müller-Dethlefs, *J. Electron Spectrosc. Relat. Phenom.*, 2000, **108**, 1.
41 A. Armentano, M. Riese, M. Taherkhani, M. B. Yezzar, K. Müller-Dethlefs, M. Fujii and O. Dopfer, *J. Phys. Chem. A*, 2010, **114**, 11139.
42 G. Lembach and B. Brutschy, *J. Chem. Phys.*, 1997, **107**, 6156.
43 A. Armentano, *Non-covalent interactions in molecular clusters: competition between π- and H-bonding*, *PhD thesis*, University of Manchester, England, 2010.
44 M. Alberti, *J. Phys. Chem. A*, 2010, **114**, 2266.
45 J. Cerny, X. Tong, P. Hobza and K. Müller-Dethlefs, *Phys. Chem. Chem. Phys.*, 2008, **10**, 2780.
46 X. Tong, A. Armentano, M. Riese, M. B. Yezzar, S. E. Pimblott, K. Müller-Dethlefs, S. Ishiuchi, M. Sakai, A. Takeda, M. Fujii and O. Dopfer, *J. Chem. Phys.*, 2010, **133**, 154308.
47 C. E. H. Dessent, S. R. Haines and K. Müller-Dethlefs, *Chem. Phys. Lett.*, 1999, **315**, 103.
48 O. Dopfer, *Int. Rev. Phys. Chem.*, 2003, **22**, 437.
49 C. Walter, R. Kritzer, A. Schubert, C. Meier, O. Dopfer and V. Engel, *J. Phys. Chem. A*, 2010, **114**, 9743.
50 M. Miyazaki, A. Takeda, S. Ishiuchi, M. Sakai, O. Dopfer and M. Fujii, *Phys. Chem. Chem. Phys.*, 2011, **13**, 2744.
51 Y. Zhao and D. G. Truhlar, *Chem. Phys. Lett.*, 2011, **502**, 1.
52 Y. Zhao and D. G. Truhlar, *Acc. Chem. Res.*, 2008, **41**, 157.
53 M. J. T. G. W. Frisch, H. B. Schlegel, G. E. Scuseria, M. A. Robb, J. R. Cheeseman, G. Scalmani, V. Barone, B. Mennucci, G. A. Petersson, H. Nakatsuji, M. Caricato, X. Li, H. P. Hratchian, A. F. Izmaylov, J. Bloino, G. Zheng, J. L. Sonnenberg, M. Hada, M. Ehara, K. Toyota, R. Fukuda, J. Hasegawa, M. Ishida, T. Nakajima, Y. Honda, O. Kitao, H. Nakai, T. Vreven, J. A. Montgomery, Jr., J. E. Peralta, F. Ogliaro, M. Bearpark, J. J. Heyd, E. Brothers, K. N. Kudin, V. N. Staroverov, R. Kobayashi, J. Normand, K. Raghavachari, A. Rendell, J. C. Burant, S. S. Iyengar, J. Tomasi, M. Cossi, N. Rega, N. J. Millam, M. Klene, J. E. Knox, J. B. Cross, V. Bakken, C. Adamo, J. Jaramillo, R. Gomperts, R. E. Stratmann, O. Yazyev, A. J. Austin, R. Cammi, C. Pomelli, J. W. Ochterski, R. L. Martin, K. Morokuma, V. G. Zakrzewski, G. A. Voth, P. Salvador, J. J. Dannenberg, S. Dapprich, A. D. Daniels, Ö. Farkas, J. B. Foresman, J. V. Ortiz, J. Cioslowski and D. J. Fox, *GAUSSIAN09, revision A.02*, Gaussian, Inc., Wallingford, CT, 2009.
54 R. Ahlrichs, M. Bär, M. Häser, H. Horn and C. Kölmel, *Chem. Phys. Lett.*, 1989, **162**, 165.
55 A. Patzer, M. Zimmermann, I. Alata, C. Jouvet and O. Dopfer, *J. Phys. Chem. A*, 2010, **114**, 12600.
56 M. F. Rode, A. L. Sobolewski, C. Dedonder-Lardeux, C. Jouvet and O. Dopfer, *J. Phys. Chem. A*, 2009, **113**, 5865.
57 C. M. Western, *PGOPHER (version 7.1.108), A Program for Simulating Rotational Structure*, University of Bristol, UK, http://pgopher.chm.bris.ac.uk.
58 P. R. Herman, P. E. Larocque and B. P. Stoicheff, *J. Chem. Phys.*, 1988, **89**, 4535.
59 E. J. Bieske, A. S. Uichanco, M. W. Rainbird and A. E. W. Knight, *J. Chem. Phys.*, 1991, **94**, 7029.
60 S. Douin, P. Parneix, F. G. Amar and P. Bréchignac, *J. Phys. Chem. A*, 1997, **101**, 122.
61 E. J. Bieske, M. W. Rainbird, I. M. Atkinson and A. E. W. Knight, *J. Chem. Phys.*, 1989, **91**, 752.
62 A. Armentano, X. Tong, M. Riese, S. E. Pimblott, K. Müller-Dethlefs, M. Fujii and O. Dopfer, *Phys. Chem. Chem. Phys.*, 2011, **13**, 6071.
63 O. Dopfer, G. Reiser, K. Müller-Dethlefs, E. W. Schlag and S. D. Colson, *J. Chem. Phys.*, 1994, **101**, 974.
64 N. Solcà and O. Dopfer, *Chem.–Eur. J.*, 2003, **9**, 3154.
65 O. Dopfer, *J. Phys. Chem. A*, 2000, **104**, 11693.
66 O. Dopfer and K. Müller-Dethlefs, *J. Chem. Phys.*, 1994, **101**, 8508.